The role of the outer mitochondrial membrane protein porin in cell death and ageing

A thesis submitted to the University of Kent for the degree of

MSc. Cell Biology

2019

Elizabeth Edrich

School of Biosciences

I DECLARATION

No part of this thesis has been submitted in support of an application for any degree or qualification of the University of Kent or any other University or institute of learning.

Elizabeth Edrich

II ACKNOWLEDGEMENTS

I would like to thank my supervisor Dr. Campbell Gourlay of the University of Kent Biosciences. He has offered me endless support and guidance throughout this project and without his vast knowledge this study would not have been possible. My gratitude also goes to Dr. Patrick Rockenfeller and Dr. Oskar Knittelfelder for providing their data, which has been of great interest.

I would also like to thank the entirety of the Kent Fungal Group, including both staff and PhD students as they have all supported me immensely and have always been prepared to help me with any questions or problems I have had over the duration of this project, namely the entire Gourlay lab.

Finally, I would like to thank my family for their continuous encouragement and support.

III CONTENTS

I Declaration 2

II Acknowledgements. 3

III Contents 4

IV List of Figures 7

V Abbreviations 9

VI Abstract 11

1. Introduction 12

1.1 VDAC structure, function and evolution 12

1.1.2 Signalling and functionality of the channel 13

1.1.3 Signalling of yeast VDAC 14

1.1.4 A debate: Is VDAC part of the mPTP? 14

1.2 Porin in neurodegeneration 15

1.3 Porin in apoptosis 16

1.4 Mitochondrial morphology, contact sites and ERMES 17

1.4.1 Lipid shuttling through ERMES 18

1.5 Autophagy in yeast 19

1.5.1. Autophagy related proteins 20

1.5.2 AMPK and autophagy 22

1.6 Mitophagy and cell wall integrity 22

1.7 Project aims 23

2. Materials and Methods 25

2.1 Growth media for S. cerevisiae 25

2.1.1 Strain inoculation and transformation 26

2.1.2 Plasmid purification from E. coli 27

2.1.3 Growth assays 28

2.2 Respirometry assays 29

2.3 Microscopy 30

2.3.1 Observation of GFP using fluorescence microscopy 30

2.3.2 Observation of cell compartments using fluorescence microscopy 30

2.3.2.1 FM4-64 staining of vacuolar membranes 30

2.3.2.2 Quinacrine staining of yeast vacuoles 30

2.3.2.3 LD540 staining of lipid droplets 31

2.4 Western blotting..... 31

2.4.1 ATG8-GFP autophagy assay..... 31

2.4.2 Whole cell protein extraction (all samples) 31

2.4.3 Preparation of polyacrylamide gels..... 32

2.4.4 SDS-PAGE gel electrophoresis..... 33

2.4.5 Semi-dry protein transfer..... 33

2.4.6 Western blot detection using Enhanced Chemiluminescence (ECL) 33

2.4.7 Antibodies used for protein detection..... 34

2.5 Flow cytometry to detect PI as a marker of necrosis..... 35

2.5.1 Flow cytometry of cells in rich and selective media..... 35

2.5.2 Flow cytometry of cells in selective media..... 35

2.6 Standards for lipid quantification performed by Dr Patrick Rockenfeller (University of Graz) and Dr. Oskar Knittelfelder (Max Planck Institute of Molecular Cell Biology and Genetics (MPI-CBG) Dresden, Germany..... 35

2.6.1 Lipid extraction and quantification by shotgun mass spectrometry..... 36

3. Results..... 38

3.1 Loss of POR1 leads to a change in mitochondrial morphology..... 38

3.2 Loss of porin leads to a loss of respiration..... 39

3.3 Growth patterns of wild-type and Δpor1 cells..... 41

3.3.1 Loss of porin stunts cellular growth..... 41

3.3.2 The growth defect displayed by Δpor1 cells can be rescued by re-expression of POR1..... 44

3.4 Autophagy in wild-type and Δpor1 cells..... 47

3.4.1 Cells lacking porin exhibit reduced levels of autophagy..... 47

3.4.2 Vacuole morphology and acidification are not affected by the loss of POR1... 50

3.5 Lipidomics of wild-type and Δpor1 cells..... 51

3.5.1 Δpor1 cells exhibit a different composition of lipids in their cell wall..... 51

3.5.2 Loss of POR1 leads to an increase in peroxisome number..... 54

3.6 Cells lacking POR1 have a higher tendency to necrose in rich media..... 56

3.7 Overexpression of POR1..... 59

3.7.1 Porin overexpression leads to an increase in necrosis..... 59

3.7.2 Flocculation and Cell Wall Integrity pathway activation occurs when porin is overexpressed…… 60

3.7.3 Cells that overexpress porin lack vacuolar integrity and may have an endocytosis defect…… 62

4. Discussion…… 62

4.1 Loss of porin leads to a change in mitochondrial morphology and loss of respiration…… 63

4.2 Both loss and overexpression of POR1 results in growth defects and necrosis 63

4.3 Cells lacking porin exhibit lower autophagy levels and altered lipidomics…….. 64

4.4 Loss of POR1 leads to increased lipid storage and peroxisome number…….. 65

4.5 Overexpression of porin leads to increased components of the Cell Wall Integrity pathway…….. 66

4.6 Final remarks and future directions…… 67

5. References…… 69

IV LIST OF FIGURES

Figure 1-1: *The structure of human VDAC1*..... 12

Figure 1-2: *The ERMES complex*..... 18

Figure 1-3: *The role of Atg1 in Atg recruitment and autophagosome formation*..... 20

Figure 1-4: *The switch between the Cvt pathway and the autophagosome pathway*..... 21

Figure 3-1: *The mitochondrial morphology of wild-type and Δpor1 cells*..... 38

Figure 3-2: *Respirometry assays of wild-type and Δpor1 cells during stationary phase*..... 40

Figure 3-3: *Growth assays of wild-type and Δpor1 cells grown in YP media*..... 42

Figure 3-4: *Growth assays of wild-type and Δpor1 cells grown in selective media*..... 43

Figure 3-5: *Summary of the exponential growth rates of wild-type and Δpor1 cells*..... 44

Figure 3-6: *Growth assays of porin overexpression strains in selective media*..... 45

Figure 3-7: *Summary of the exponential growth rates of wild-type and Δpor1 cells*..... 46

Figure 3-8: *Observation of autophagy efficiency in wild-type and Δpor1 cells*..... 48

Figure 3-9: *Western blot showing the levels of ATG8-GFP in both wild-type and Δpor1 cells*..... 49

Figure 3-10: *Vacuole structure of wild-type and Δpor1 cells*..... 50

Figure 3-11: *Vacuole acidity of wild-type and Δpor1 cells*..... 50

Figure 3-12: *Lipid composition of the cell wall of S. cerevisiae*..... 51

Figure 3-13: *Cell wall thickness of wild-type and Δpor1 cells*..... 52

Figure 3-14: *Observation of lipid droplets in wild-type and Δpor1 cells*..... 53

Figure 3-15: *Lipid droplet number of wild-type and Δpor1 cells*..... 54

Figure 3-16: *Visualisation of peroxisomes in wild-type and Δpor1 cells*..... 55

Figure 3-17: *Peroxisome number of wild-type and Δpor1 cells*..... 55

Figure 3-18: *Graph displaying the necrosis levels of wild-type and Δpor1 cells in YPD media* 56

Figure 3-19: *Graphs displaying the necrosis levels of wild-type and Δpor1 cells in synthetic media*..... 58

Figure 3-20: *Western blot showing the levels of porin in S. cerevisiae*..... 59

Figure 3-21: *Graph displaying the necrosis levels of cells that overexpress porin in SD-URA* 60

Figure 3-22: *Overnight cultures of cells that overexpress porin show flocculation……* 61

Figure 3-23: *Western blot showing the levels of phosphorylated Slt2 in cells that overexpress porin……* 61

Figure 3-24: *Vacuolar structure of cells containing a porin overexpression plasmid……* 62

Figure 4-1: *Schematic illustrating the potential roles of porin……* 67

V ABBREVIATIONS

AIM	Atg8-family Interacting Motifs
AMPK	AMP Activated Kinase
AntA	Antimycin A
Atg	Autophagy Related proteins
CDP-choline	Cytidine 5'-Diphosphocholine
CL	Cardiolipin
Cvt	Cytoplasm to Vacuole Targeting
CSM	Complete Supplement Media
CWI	Cell Wall Integrity Pathway
ECL	Enhanced Chemiluminescence
ERMD	ER-Mitochondrial Division
ERMES	ER-Mitochondria Encounter Structure
FACS	Fluorescence-Activated Cell Sorter
GFP	Green Fluorescent Protein
GlpD	Glycerol-3-Phosphate Dehydrogenase
HPFE	High Pressure Freezing and Embedding
HPLC	High-Performance Liquid Chromatography
IMM	Inner Mitochondrial Membrane
LiOAc	Lithium Acetate
LIR	LC3- Interacting Region
MAM	Mitochondrial Associated ER Membrane
mERs	Mitochondrial Oestrogen Receptors
MFQL	Molecular Fragmentation Query Language
mPTP	Mitochondrial Permeability Transition Pore
MtCK	Mitochondrial Creatine Kinase
mtDNA	Mitochondrial DNA
NS	Nitrogen Starvation
OMM	Outer Mitochondrial Membrane
PAS	Pre-Autophagosomal Structure
PBS	Phosphate Buffered Saline

PBS/T	PBS + Tween 20
PC	Phosphatidylcholine
PE	Phosphatidylethanolamine
PEG	Polyethylene Glycol
PI	Potassium Iodide
PRM	Parallel Reaction Monitoring
PS	Phosphatidylserine
PVDF	Polyvinylidene Difluoride
ROS	Reactive Oxygen Species
RPM	Revolutions Per Minute
SAM	Sorting and Assembly Machinery
SC	Synthetic Complete
SD	Synthetic Defined
SDS-PAGE	Sodium Dodecyl Sulfate–Polyacrylamide Gel Electrophoresis
SOD	Superoxide Dismutase
TEM	Transmission Electron Microscopy
TEMED	Tetramethylethylenediamine
TET	Triethyltin Bromide
TOM	Translocase of the Outer mitochondrial Membrane
ULK1	Unc-51-like kinase 1
VDAC	Voltage-dependent Anion channel

VI ABSTRACT

The Outer Mitochondrial Membrane (OMM) contains channels to regulate metabolic flux, such as the Voltage-Dependent Anion Channel (VDAC) also referred to as porin in *Saccharomyces cerevisiae*. Porin has been reported to play a role in apoptosis and oxidative stress, but surprisingly little is known about the role of VDAC in mitochondrial morphology, mitophagy, autophagy or ER-mitochondria connections (The ER-mitochondria encounter structure, ERMES). We present evidence through fluorescence microscopy that porin1 is associated with the ERMES complex and that its deletion results in aggregation of mitochondria that mimics the loss of ERMES components. This aggregation is associated with a loss of respiration, reduced capacity for autophagy, an increase in peroxisome number and elevated necrosis, elucidated through respirometry assays, western blots and flow cytometry. We have also found that overexpression of porin leads to activation of the cell wall integrity pathway, flocculation and vacuole fragmentation. Our experiments suggest that porin plays a critical role in the maintenance of mitochondrial function and the regulation of several important signalling mechanisms. These functions may be linked to as yet undefined roles for porin in lipid metabolism and the assembly of stress regulatory complexes on the mitochondrial surface.

1. INTRODUCTION

Cells rely on the selective permeability of mitochondrial membranes for a variety of functions. While mitochondria in *Saccharomyces cerevisiae* are most commonly known for their integral role in cellular metabolism, the control and permeability of both the inner and outer membranes is vital for apoptosis and cellular ageing[1]. Channels found in the Outer Mitochondrial Membrane (OMM) include the Voltage-Dependent Anion Channel (VDAC) also referred to as porin in yeast. Porin is the most abundant protein in the OMM, forming up to 50% of the proteins found in the OMM of *Neurospora crassa* [2,3] – reflecting its importance in mitochondrial functions.

1.1 VDAC structure, function and evolution

Following the discovery of porin in *Paramecium aurelia* in 1976[4], many studies have elucidated the structure and overall function of this channel.

The voltage-gated anion channel has three isoforms, all of which reside in the OMM; VDAC1, VDAC2 and VDAC3, ranging between 29 to 37 kDa[5,6]. The structure of VDAC1 is highly conserved[7] and consists of a β-barrel containing 19 amphipathic β-strands and an N-terminus formed of α-helical segments (*Figure 1-1*), which seems to wedge into the channel and partially block it[2,8,9].

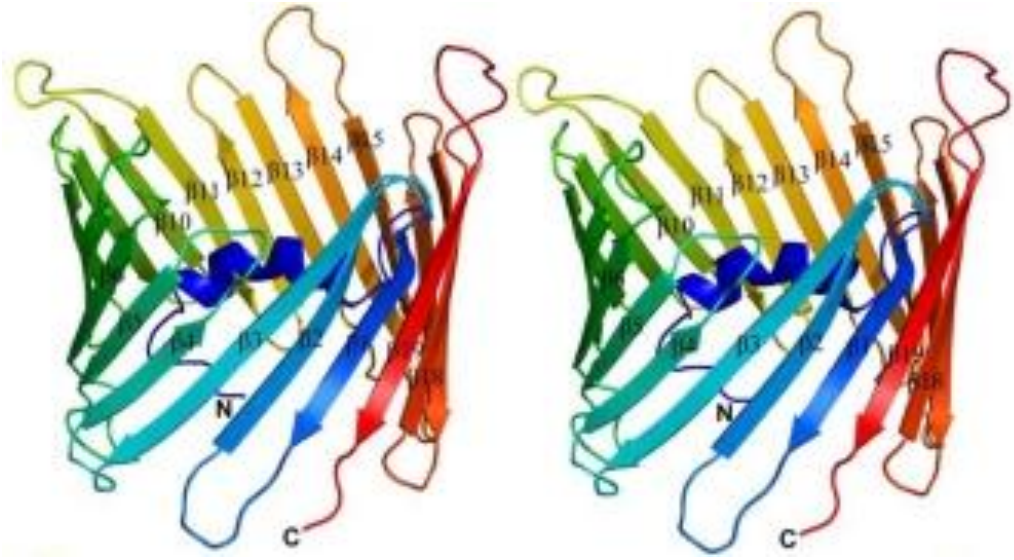


Figure 1-1: The structure of human VDAC1.
Derived from Bayrhuber et. al [2] whereby the channel measures ~3.5 x 3.1 nm in the horizontal and ~4nm in the vertical direction.

While VDAC1 shows high levels of evolutionary conservation across metazoans, plants and fungi[7], studies have noted that the number of isoforms present denotes how complex the organism is. Higher eukaryotes typically possess all three VDAC isoforms[7], although each isoform has different abilities. VDAC1 and VDAC2 can insert easily into phospholipid membranes but VDAC3, commonly found in spermatozoa[10], has a drastically reduced pore forming ability[11]. This may be due to the different cysteine residue dispositions, where VDAC1 has 2 cysteines, VDAC3 has 6 cysteines and VDAC2 has 9 in humans[5]. Because cysteines are involved in redox modifications and disulphide bridges, the positioning of the residues within VDAC isoforms will determine the activity that each one can have. For example, the two cysteines of VDAC1 (Cys232 and Cys127) protrude into both the interior and the hydrophobic section of the channel, respectively[5].

Elegant studies by Reina et. al[5] demonstrated that different VDAC isoforms have slightly different N-terminal sequences. For example, VDAC2 has two extensions of the N-terminus, while VDAC3 has an N-terminus with very little activity[5]. Swapping the N-terminus of VDAC1 with VDAC3 allowed the resulting channel (N1-VDAC3) to resist oxidation and increase the cell lifespan by 50%[5]. This indicates that N-terminal properties associated with specific VDAC isoforms dictates the functional activity of the channel. It should be noted that dynamic instability of the N-terminal has been elucidated as critical for channel function by Bayrhuber et.al[2], who demonstrated that a conserved Glu-73 residue in the N-terminus is vital for its interaction with cytoplasmic proteins such as Hexokinase-1 and Ruthenium Red[2]. One could speculate, therefore, that different VDAC isoforms may have roles in multiple signalling pathways.

1.1.2 Signalling and functionality of the channel

As the name suggests, VDAC is an anion channel which allows the passage of many metabolites between the mitochondrial intermembrane space and the cytoplasm, thus acting as a controller of metabolic flux[12-14]. Numerous studies have shown that VDAC is directly involved in the regulation of apoptosis, ATP flux, oxidative stress mediation and Ca2+ homeostasis[15-19]. Interestingly, Bera et. al[20] noted that VDAC has a 'dual' system; that is, it has both open and closed states that can act according to the mitochondrial membrane potential and dictate the activity of the channel. This

idea of voltage gating is supported by Rostovtseva et.al[17] and Karachitos et.al[18] who deemed the 'open' state of VDAC to be 3.9 nanoseconds (nS) at a membrane potential of +10mV, and the 'closed' state to be 2.6 – 2.2 nS between +40 and +70mV[18]. It is this voltage gating that permits VDAC to be a useful filter for mitochondrial permeability. However, although porin transports anions, studies by Gurnev et. al[21] demonstrate that tubulin can block the VDAC pore with its negatively charged tail, and in doing so changes the selectivity of VDAC to cationic, differing from the 'open' state[21]. This evidence indicates that although porin has a 'dual' mode of action, the functionality of the channel itself can in part be influenced by cytosolic binding partners.

1.1.3 Signalling of yeast VDAC

In *S. cerevisiae*, porin1 has been shown to interact with several proteins, including those that facilitate its insertion into the OMM. A study by Krimmer et. al[22] noted that key interactions in this process rely on the Translocase of the Outer mitochondrial Membrane (TOM) complex, namely Tom22 (the central receptor), Tom40, Tom7 and Tom5[22]. This evidence is supported by Kozjack-Palovic et.al[23], who demonstrated that the Sorting and Assembly Machinery (Sam50) and metaxins are vital to the import of the porin precursor into the OMM, through interaction with TOM complexes[23]. Interestingly, these import proteins are affected by the levels of Superoxide Dismutase (SOD) in the cell. One study confirmed that to prevent premature cellular aging, Copper-and-Zinc containing Dismutase (CuZnSOD) is vital for maintaining VDAC levels, Tom40 levels and Tob55/Sam50 levels in *S. cerevisiae*[18]. This is because SOD protects VDAC from oxidation by O_2^- and prevents porin channel closure[18]. However, if SOD is absent and VDAC levels fall because of oxidative damage, it is tempting to speculate that the levels of the TOB/SAM complexes could increase to enhance VDAC import. This evidence shows the pivotal role that VDAC has in maintaining the lifespan of the cell in conjunction with oxidative stress.

1.1.4 The debate: Is porin part of the mPTP?

Some studies have claimed that porin is part of the Mitochondrial Permeability Transition Pore mPTP[24-27] - known for cytochrome *c* release and caspase activation. For example, Veenman et. al[27]

claimed that VDAC is the central component of the mPTP, where TSPO binds to porin to open the mPTP and induce apoptosis via Reactive Oxygen Species (ROS) production[27]. Supporting the idea that VDAC is a central part of the mPTP, a study by Schlattner et. al[28] demonstrated that porin is a receptor for mitochondrial creatine kinase (MtCK), an interaction that is enhanced by calcium. This study postulates that MtCK binding may interfere not only with the mPTP, but with the initiation of apoptosis through VDAC[28]. However, this idea is debated as there is little evidence to directly link the channel as part of the complex itself. For example, studies including those by Baines et.al[29] agree that VDAC is dispensable in this case; that is, porin cannot be a main constituent of the mPTP as removal of VDAC does not drastically hinder the ability of the mPTP to function. In fact, several studies[30-32] including those by Nakagawa et. al[33] and Nesci et. al[34] have demonstrated that Cyclophilin D and the F1F0-ATPase are the only core constituents of the mPTP. This evidence suggests that VDAC may directly influence the other components of the mPTP to control the permeability of the outer membrane in multiple ways but is not necessarily a core component in this structure.

1.2 Porin in neurodegeneration

VDAC has been linked to neurodegenerative diseases such as Parkinson's and Alzheimer's disease[5]. For example, studies suggest that VDAC may play a role in neurotoxicity, as it is found in a complex with oestrogen receptors (mERs) which in turn forms lipid rafts in several areas of the brain[35,36]. Interestingly, acrolein, thought to be causative of Alzheimer's, is known to induce a 13-fold oxidation of porin sidechains (carbonylation)[5,37]. This was supported by another study by Cuadrajo-Tejedor[38], which showed that there was a correlation between levels of amyloid-β peptide and increased levels of VDAC1 in the hippocampus of Tg2576 mice[38]. This evidence presents a strong case for the involvement of porin in neurodegeneration. Furthermore, studies by Sun[39] indicated that VDAC serves as a docking port for functioning Parkin to induce mitophagy. It is tempting to speculate, therefore, that while mutations in Parkin and its translocator PINK1 are implicated in Parkinson's disease, porin may also be directly affected or mutated in this case.

1.3 Porin in apoptosis

In apoptosis, pro-apoptotic proteins such as Bax, Bid, Bim, and Bak translocate to the mitochondria, where they initiate the release of Smac/Diablo and cytochrome *c.* However, some studies suggest that mammalian isoforms of VDAC are involved directly in this process. For example, Shimizu et.al[40] and Sugiyama et. al[41] suggest that VDAC binds directly to Bax Bak, and Bim, but the BH3 only protein Bid did not depend on mVDAC binding for apoptosis. Further studies that introduced Bim and Bcl-2 into yeast, which acted as a model system and confirmed that Bim was able to induce cytochrome *c* release in the absence of other Bcl-2 family proteins[41], indicating that this is an essential signalling pathway in mammalian cells. Similarly, Yuan et.al[42] demonstrated that VDAC1 was involved in endothelial cell apoptosis through interactions with endostatin. This study speculates that endostatin sensitises cells to apoptosis through opening of the mPTP via an interaction with VDAC1[42]. This, in turn, reduces hexokinase II binding which promotes VDAC phosphorylation and prevents its degradation. While these studies support the idea of porin being an initiator of apoptosis, Chen et. al[43] claims that Nek1 keeps cells alive after DNA damage through phosphorylation of VDAC1. This evidence indicates that porin is a dynamic regulator of apoptosis that can have dual signalling roles, depending on its phosphorylation state.

While porin shows multiple binding pathways and dual signalling roles in regulating apoptosis, studies have confirmed that hexokinases such as HKI and HKII bind to VDAC to prevent apoptosis. Abu-Hamad et.al[44] showed that VDAC1 has two cytosolic loops that are responsible for binding to hexokinase-I, one of which contains a Glu-72 residue and one contains a Glu-202 residue[44]. The binding of HKI to these residues is vital for inhibition of cytochrome *c* release, whereby the Glu-202 residue stabilises the interaction of HKI with Glu-72[44]. Interestingly, this Glu-72 loop has been isolated in other studies as a voltage sensor in *Neuraspora crassa* and yeast[45,46], indicating that this residue is vital for VDAC functionality. Further phosphorylation of VDAC by GSK3β interrupts the binding of hexokinases to the mitochondria[38], which supports the idea that the phosphorylation state of porin influences its function. It could be postulated that the Glu-73 residue of VDAC, isolated by Bayrhuber et. al[2] as being vital for N-terminal dynamic instability, could also be involved

in HKI binding through increased flexibility of the channel N-terminus.

While we know apoptosis and cytochrome *c* release from the mitochondria is dependent on porin phosphorylation, formation of porin oligomers in the OMM could act as an extra signal for apoptotic pathways. Studies have used bioluminescence and crystallisation experiments[16,47] to observe the formation of VDAC oligomers through cross linking in the mitochondrial membrane, which not only increases the levels of caspase 9, but also initiates the production of ROS[16,47,48]. This evidence indicates that the dynamic and conformational changes resulting from porin oligomerisation creates an apoptotic signal and can change the conductance states of the channel.

1.4 Mitochondrial morphology, contact sites and ERMES

While we have seen that porin plays an essential role in apoptosis and oxidative stress, surprisingly little is known about the role of porin in mitochondrial morphology, mitophagy, autophagy or ER-mitochondria connections in yeast (the ER-mitochondria encounter structure, ERMES[49]). While some mechanisms behind ER-mitochondrial linkage are unknown, several studies have elucidated that the ERMES complex may be involved in the lipid exchange between these two organelles in yeast[49-52] as lipid metabolism in higher eukaryotes is facilitated through Mitochondrial Associated ER Membranes (MAMs)[50].

In yeast, ERMES is composed of four proteins: An ER protein Mmm1, a cytosolic protein Mdm12, Mdm10, which is a β-barrel OMM protein, and Mdm34[49,51] (*Figure 1-2)*. While Kawano et.al[52] has demonstrated that Mmm1 and Mdm12 form a complex that specifically mediates lipid translocation, Mdm10 has been shown to interact with SAM, in order to assist with construction of Tom40[53,54]. Yamano et. al[54] demonstrated that because Mdm10 is a β-barrel itself, it may compete with other β-barrels for binding with SAM. It is tempting to speculate, therefore, that porin could be involved in this competitive binding.

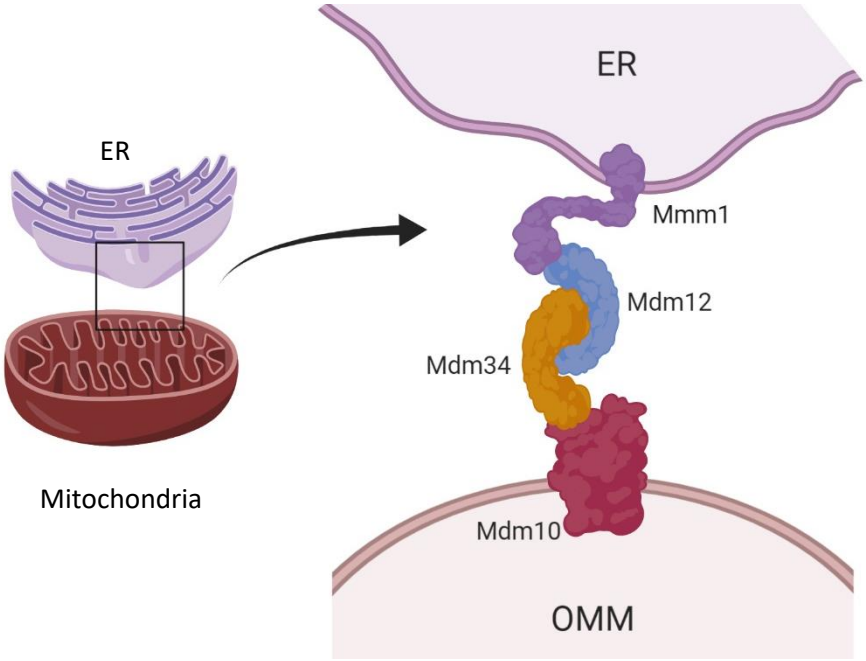


Figure 1-2: The ERMES complex. A basic diagram depicting an ER-mitochondrial connection through the ERMES complex. ER = Endoplasmic Reticulum. OMM = Outer Mitochondrial Membrane. Created with BioRender.com.

ERMES has also been implicated in mitochondrial fission and division, known as ER-associated Mitochondrial Division (ERMD)[50,55]. Mitochondrial division has been shown to occur at ER-mitochondria contact sites[55] and ERMES null or mutant cells show an odd mitochondrial morphology in yeast[56,57]. Mutant VDAC mirror this change in mitochondrial morphology as mutations in VDAC lead to mitochondrial elongation and overexpression of VDAC resulted in fragmented mitochondria in *Drosophila*[58]. These studies indicate that VDAC may be critical for functional mitochondrial morphology and maintenance of ERMES connections.

1.4.1 Lipid shuttling through ERMES

While ERMES physically connects the ER and the mitochondria, Kawano et.al[52] have shown that Mmm1 and Mdm12 specifically mediates efficient lipid transfer between the two organelles. Because mitochondria and the ER in yeast are required to synthesize glycerophospholipids[49], ERMES connection sites are thought to play a major role in lipid maturation and production of essential cellular molecules. Pertinent examples are phospholipids such as Phosphatidylserine (PS), which originate in the ER and are consequently shuttled to the mitochondria to be decarboxylated by Psd1[59]. The product of this decarboxylation in the mitochondria is Phosphatidylethanolamine (PE)[60,61] which is the major source of cellular PE[62]. Any PE not utilised by the cell is shuttled back to

the ER to be methylated into Phosphatidylcholine (PC)[61]. Achleitner et.al[60] confirmed that MAMs play an integral role in this lipid shuttling. However, some lipids synthesised through the ER-mitochondrial connections are not widely distributed within the cell; for example, Cardiolipin (CL) is a phospholipid that has a 25% abundance in the OMM[63] but has a synthase enzyme in the IMM[64]. The importance of CL is reflected in a study by Gohil et.al[65], who confirmed that cells lacking CL must rely on mitochondrial synthesis of PE to remain viable. This could be because CL may be important for mitochondrial membrane structure[64]. These studies highlight the functional importance of ERMES not only for organelle structure but for synthesis and distribution of important cellular lipids.

1.5 Autophagy in Yeast

Studies have concluded that VDAC is linked to Autophagy, a highly regulated process in which cytoplasmic contents including damaged organelles are hydrolysed to maintain energy homeostasis. This is a process that, in yeast, is often in response to nutrient starvation. Although bulk autophagy is most common in nutrient starvation conditions, there are many types of selective autophagy, such as mitophagy, ribophagy, the degradation of ribosomes[66] and the degradation of peroxisomes, termed pexophagy[67,68]. In mitophagy, VDAC recruits Parkin to defective mitochondria[69], although its role in other types of autophagy is unclear. Autophagy is often linked to cytoplasm to vacuole targeting (Cvt) in yeast, and the autophagic machinery has been well documented in *S. cerevisiae,* particularly for autophagosome construction[70]. However, it should be noted that the Cvt pathway is constitutive; that is, autophagic pathways only occur during nutrient depravation, but Cvt can occur at any time[71].

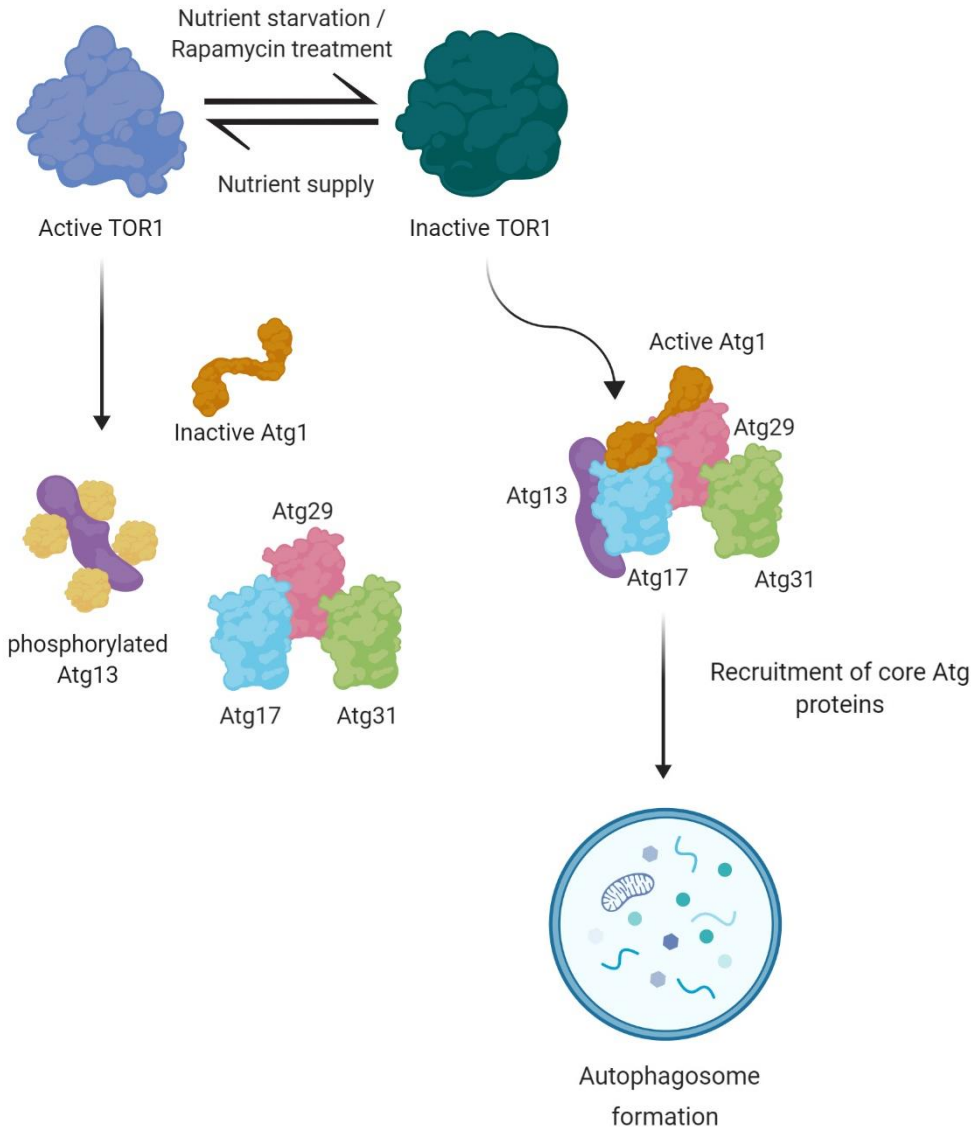


Figure 1-3: The role of Atg1 in Atg recruitment and autophagosome formation.
When TOR1 is active, Atg13 remains phosphorylated and Atg1 is therefore inactive. Under nutrient starvation, (or Rapamycin treatment) Atg1 is activated and can conjugate with other Atg proteins to promote autophagosome formation. Adapted from Nakatogawa et. al [81] and created with BioRender.com.

1.5.1. Autophagy related proteins

Autophagy in yeast involves autophagy related proteins (Atg) such as Atg8, which is heavily involved in regulation of autophagosome size and formation[72]. One of the most crucial Atg proteins in yeast is Atg1, which has the mammalian homologue ULK1 (Unc-51-like kinase 1)[73]. Under nutrient starvation (*Figure 1-3)*, the kinase activity of Atg1 is increased through phosphorylation[74], whereby Atg1 consequently interacts with Atg13, Atg17, Atg29 and Atg31[75-77]. This resultant complex is thought to play a role in autophagosome formation[75], which can also be induced in

yeast and mammalian cells through the presence of Rapamycin. Under nutrient stress, or when Rapamycin is present, yeast TOR is inhibited, which dephosphorylates Atg13 and thus promotes the Atg1-Agt13-Atg17 interaction[75,76]. Atg1 also works to retrieve Atg23 and Atg9 from the Pre-Autophagosomal Structure (PAS)[78,79]. Because of its critical role in nutrient signalling pathways, Mizushima et. al[80] has suggested that Atg1 may be a switch between the Cvt and autophagic pathways in yeast, depending on nutrient availability - a concept visualised in *Figure 1-4.* This is because while Atg1 plays a central role in autophagosome formation and PAS organisation for autophagy, it can also play a role in the Cvt complex by mediating Cvt vesicle formation via PAS recruitment[81,82].

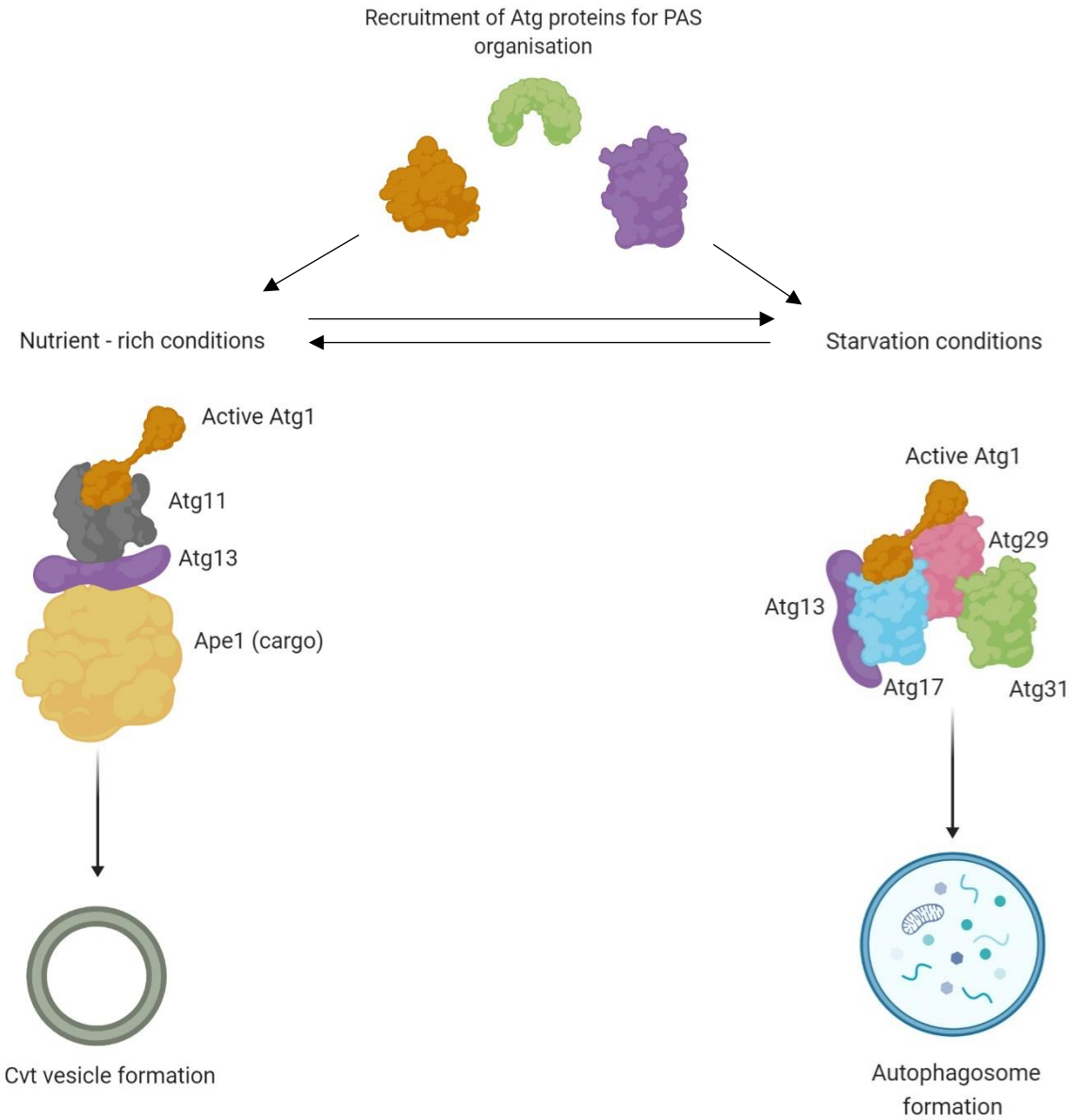


Figure 1-4: The switch between the Cvt pathway and the autophagosome pathway.
The switch between Cvt vesicle formation and autophagosome formation is based on nutrient availability. Adapted from Mizushima et. al[80] and created with BioRender.com

1.5.2 AMPK and autophagy

The homolog of the AMP Activated Kinase (AMPK)[83] in yeast, SNF1[84], monitors extracellular levels of glucose and regulates gene expression accordingly. When glucose levels are limiting, SNF1 is activated through phosphorylation of Thr120 and Thr127 within its active T-loop via ADP and AMP[85,86]. This active form of SNF1 is protected from dephosphorylation by Glc7 via ADP binding at two distinct sites[84]; one of which is localised on the γ-subunit (snf4), which is structurally exclusive to *S. cerevisiae*[87]. The consequential active form of SNF1/AMPK then allows Atg1 activation through phosphorylation of Ser317 and Ser777 via the AMP-activated Kinase (AMPK)[83,88]. SNF1 also promotes the phosphorylation of Atg6 and inhibits TOR in order to initiate autophagy[89].

Interestingly, Yi et. al[90] elegantly demonstrated that SNF1 forms a complex with Mec1 and Atg1 on mitochondrial surfaces during glucose starvation. This study suggests that under glucose starvation, SNF1 and Mec1 are recruited to the mitochondrial membrane (but not PAS markers), whereby Mec1 is specifically recruited by Ggc1[90]. Mec1, a DNA-damage response protein, is phosphorylated at T797, T1074 and S552 by SNF1 on the mitochondria after recruitment by Ggc1[90]. This phosphorylation, in turn, recruits Atg1 and Atg13 to the mitochondrial membrane. The SNF1-Mec1-Atg1 complex is essential for mitochondrial respiration under glucose starvation conditions[90]. However, how certain parts of these pathways interact is still unclear. While Mec1 is recruited to the mitochondria by Ggc1, studies have shown that the localisation of Ggc1 is in the IMM[91], indicating that an OMM partner may be required for Mec1 recruitment or complex formation. It would be tempting to suggest, therefore, that porin may be involved in connecting and monitoring this complex formation and so a loss of porin would result in a lack of mitochondrial respiration under starvation conditions.

1.6 Mitophagy and cell wall integrity

Mitophagy, a type of selective autophagy, is used by cells to remove damaged mitochondria and avoid cell death. Mitophagy is often brought on by the effects of oxidative stress, including ROS production and calcium ion overload. It would be logical to postulate that mitophagy would be a

consequence of porin dysfunction, as porin acts as the gating mechanism for relief of oxygen radicals from the mitochondria and calcium homeostasis. However, the role of porin in mitophagy is yet to be elucidated. Because mitophagy is used to remove damaged mitochondria, mutations in the mechanisms of this process could drastically reduce the lifespan of the cell.

Mitophagy is thought to be linked to two MAPK pathways; the Hog1 activated pathway and the Slt2 activated pathway[92]. Both signalling pathways are involved in the Cell Wall Integrity pathway (CWI) and hyper osmotic stress response, respectively[93,94]. Mao et. al[92] demonstrated not only that Hog1 and Slt2 are involved in mitophagy, but it has been shown that they are involved in the Ssk1-Pbs2-Hog1-CK2 and Wsc1-PKC1-Bck1-Mkk1/2-Slt2 pathways[92,95]. Through Atg32 recruitment to PAS, this study showed that while Hog1 is mitophagy specific and occurs in later stages, Slt2 may be involved earlier in mitophagy and could also play a role in pexophagy[92]. Mitophagy factors in yeast such as Atg32, Atg11 and Atg8 also play a vital role in mitochondrial targeting to PAS, whereby Atg32 is thought to be a mitochondria specific receptor that mediates mitochondrial degradation in this case[96,97]. Atg32 can interact with Atg11, an adaptor protein which also plays a role in the Cvt pathway[98]. It appears that when mitophagy is induced, phosphorylation of Ser114 and Ser119 on Atg32 mediates the interaction of the Atg11 C-terminus and the N-terminus of Atg32, which in turn is related to Pbs2 and Hog1[99]. Atg32 can also interact with Atg8 via the LC3-Interacting Region (LIR) and Atg8-family Interacting Motifs (AIM)[100]. Studies by Kaufmann et. al have shown that Atg8 can also bind to PE, which allows Atg8 to also conjugate with Atg5, Atg12 and Atg16 and forms a scaffold[101,102]. It would be tempting to speculate, therefore, that the known pathways of mitophagy could be linked through porin to mediate mitochondrial degradation.

1.7 Project Aims

In this study, we investigate the roles of the Voltage Dependent Anion Channel, porin1, in mitochondrial morphology and function and investigate how this affects cellular ageing and death. This was done using six key objectives:

1. Analysis of mitochondrial morphology in wild-type and porin mutant cells
2. Analysis of porin importance in cell nutrition and health in response to different stresses such as a change in carbon source.
3. Conduct respirometry and chronological ageing assays to determine whether the effects of porin on mitochondrial morphology affects mitochondrial function and cellular ageing.
4. Observation of autophagy in porin mutant cells and identification of any changes in signalling pathways as a result of mitochondrial dysfunction.
5. Analysis of necrosis patterns of porin mutant cells.
6. Analysis of the phenotypic and functional effects from porin overexpression in areas 1-5 and whether any phenotypes observed can be reversed through porin re-expression.

2. Materials and Methods

2.1 Growth media for S. cerevisiae

Liquid cultures of wild-type and *Δpor1 S. cerevisiae* strains were grown in either YPD (1% Yeast extract (Difco), 2% Bactopeptone (Difco) and 2% Dextrose (Fisher Scientific)) or Synthetic Defined (SD-URA) media (0.675% Yeast Nitrogen base without amino acids (Formedium), 0.193% yeast synthetic dropout Kaiser mixture without Uracil (Formedium) added as per the manufacturers' guidelines, and 2% Dextrose (Fisher Scientific)) overnight on a 30°C rotary shaker at 180 revolutions per minute (RPM). Cells that contained the porin overexpression plasmid (PCG633) and the empty vector plasmid (PCG557) were always grown on SD-URA media. Culture plates were also made to grow the strains and transformants, which contained the appropriate media with added 20% Oxoid Technical Agar (Agar No. 3).

Selective Synthetic Complete (SC) media was used for individual experiments and contained 0.675% Yeast Nitrogen base without amino acids (Formedium), 0.079% Yeast Complete Supplement Mixture (CSM) (Formedium) added as per the manufacturers' guidelines, and 2% Dextrose (Fisher Scientific). SC media was also made without Ammonium Sulphate, containing 0.17% Yeast Nitrogen base without amino acids and ammonium sulphate (Difco), 0.079% CSM (Formedium) added as per the manufacturers' guidelines, and 2% Dextrose (Fisher Scientific). Variants of SC media were made containing the same components as SC without ammonium sulphate, but with lower levels of CSM. (SC) without Ammonium Sulphate (50%) contained 0.04% CSM, and (SC) without Ammonium Sulphate (25%) contained 0.02% CSM. The components of other media used in this study can be found in *Table 2-1*.

Table 2-1: List of different media used.

Media	***Components***
Nitrogen Starvation Media (NS)	0.675% Yeast Nitrogen base without amino acids and ammonium sulphate (Difco) 0.193% yeast synthetic dropout Kaiser mixture without Uracil (Formedium) added as per the manufacturers' guidelines, and 2% Dextrose (Fisher Scientific)
YT media	1.6% Tryptone (Difco), 1% Yeast Extract (Difco), 0.5% NaCl

2.1.1 Strain inoculation and transformation

All strains of *S. cerevisiae* used in this study can be seen in *Table 2-2*. Overnight starter cultures of wild-type strains and strains with the *POR1* gene deleted (Δ*por1*) were incubated at 30°C in 5ml of YPD media. The starter cultures were then aliquoted into Eppendorf tubes and pelleted at 13000 RPM for 30 seconds, and the supernatant was discarded. The pellets were resuspended in transformation mix, which can be seen in *Table 2-3*, and heat shocked in a water bath for 45 minutes at 42°C. The mix was then pelleted again, and the resulting cells were aliquoted onto the appropriate agar selection plate followed by a three-day incubation at 30°C. Colonies were then picked and re-streaked onto fresh agar selection plates or suspended in liquid media for overnight growth.

Table 2-2: S. cerevisiae strains used in this study.

Strain	***Genotype***
CGY384	wild type strain, Matalpha *ura3-52, his3Δ200, leu2-3,112 lys2-801 COF1::LEU2*
CGY1061	Made from CGY384 Matalpha *ura3-52, his3Δ200, leu2-3,112 lys2-801 COF1::LEU2 por1Δ::HIS3*
CGY628	*MATa his3Δ1 leu2Δ0 met15Δ0 ura3Δ0* rho^{o} made from CGY424 (BY4741 wild type MATa *his3Δ1 leu2Δ0 met15Δ0 ura3Δ0)*
CGY638	MATa his3Δ1 leu2Δ0 met15Δ0 ura3Δ0 cox4::HIS3

Table 2-3: Mixture used for all transformations in this study.

Component	***Amount (µl)***
50% w/v Polyethylene Glycol (PEG) 4000	240
1M Lithium Acetate (LiOAc)	36
10mg/ml single stranded DNA (from salmon sperm)	10
Sterile MilliQ water	42
Desired plasmid (100ng/µl)	2

2.1.2 Plasmid purification from E. coli

E. coli strains were grown to obtain the plasmids used in this study. Cultures of competent cells were grown overnight at 37°C on a rotary shaker and inoculated with the desired plasmid, shaking at 180 RPM in YT media (see *Table 2-1*) with Ampicillin at 1mg/ml. A QIAprep Spin Miniprep Kit was used to extract and concentrate the desired plasmids as per the manufacturer's instructions.

Table 2-4: List of plasmids used.

Plasmid	***Description***	***Selective Marker***	***Source***
pVT100U-mtGFP	Plasmid containing an ADH promotor. Ampicillin resistant from a DH5α strain.	URA3	Benedikt Westermann[103] (Addgene plasmid # 45054; http://n2t.net/addgene:45054; RRID:Addgene_45054)
PCG636	Low copy plasmid expressing ATG8–GFP.	URA3	Professor Frank Madeo, University of Graz.
PCG633	Made by Gateway expression system. POR1 was inserted into pAG416 containing a CEN origin of replication and a GPD promoter.	URA3	CWG
PCG557	Ampicillin resistant gateway destination vector containing a GPD promoter.	URA3	Simon Alberti[104]
PCG428	Plasmid with GFP-PTS1 peroxisome targeting sequence driven by a constitutive promoter (TPI promoter)	URA3	A kind gift from Dr. Ewald Hettema (University of Sheffield)

2.1.3 Growth assays

Wild-type, *Δpor1* and Por1 overexpression strains were grown overnight in 5ml of media (YPD, SC and SD-URA), shaking in a rotary shaker at 180 RPM at 30°C. The absorbance (OD600) of the

cultures was measured on an Eppendorf Biophometer plus after overnight growth. The cultures were inoculated to a starting OD600 of 0.1 in a sterile 48 well plate (Greiner) in technical and biological triplicates. The plate was measured for 24 – 48 hours using a BMG LabTech SPECTROstar nano plate reader using the setting shown in *Table 2-5* and was analysed using MARS software. Exponential growth rates were then calculated in Excel using the log of the number of cells at time (t) minus the log of the number of cells at time zero (t_0), which equals the growth rate constant multiplied by the time interval: $\mu = ((\log_{10} N - \log_{10} N_0) 2.303) / (t - t_0)$.

Table 2-5: Measurement settings on the BMG LabTech SPECTROstar nano.

Excitation	600nm
Cycle time	360 seconds
Shaking frequency	400 RPM
Shaking Mode	8-minute linear shake followed by double orbital shaking
Temperature	30°C
Positioning Delay	0.5 seconds

2.2 Respirometry assays

To determine the oxygen consumption and capacity of wild-type and *Δpor1* strains respirometry was performed using an O2k Oxygraph (Oroboros) high resolution respirometer. A 2.5ml suspension of the cells grown in SD-URA + glucose and suspensions of the cells grown in SD-URA + glycerol was added to the Oxygraph chambers at a concentration of c.$1x10^6$ after overnight growth. A 20-minute period of cellular routine respiration was allowed to reflect the metabolic activity under cell culture conditions. 8µl of 50mM Triethyltin Bromide (TET) was added to each chamber resulting in the leak of respiration caused by compensation for the proton leak after inhibition of ATP synthase. Following the leak 2µl of 12mM FCCP was added to each chamber to uncouple the electron transport chain from the oxidative phosphorylation system through interference of the proton gradient. Finally, 2µl of 20mM Antimycin A (AntA) was added to each chamber inhibiting respiration through inhibition of complex I and II of the electron transport system[105].

2.3 Microscopy

2.3.1 Observation of GFP using fluorescence microscopy

Wild-type and *Δpor1* strains transformed with a plasmid expressing GFP were grown overnight in 5ml SD-URA at 30°C and the resulting cultures were pelleted at 4000 RPM for 5 minutes. The supernatant was discarded, and the pellets were resuspended in 200µl of SD-URA. 3µl of the resulting mixture was pipetted onto a glass slide and analysed using an Olympus IX-81 fluorescence microscope with a CooLED illumination system using 488nm excitation and 520 emission and an Olympus 100x 1.4NA Plan NeoFluor oil-immersion objective. Images were captured when the cells were in stationary and log phase using an Andor-Xyla 4.2 CMOS camera with an exposure time of 10-100ms. Images were captured, saved and processed using MicroManager and ImageJ software.

2.3.2 Observation of cell compartments using fluorescence microscopy

2.3.2.1 FM4-64 staining of vacuolar membranes

Wild-type, *Δpor1* and Por1 overexpression strains of *S. cerevisiae* were grown to exponential and stationary phase overnight in YPD and SD-URA medium respectively at 30°C in 5ml of culture. The strains were then pelleted at 8000 RPM for 1 minute and re-suspended in 500µl of YPD and FM4-64 stain added to a final concentration of 8µM. The strains were then incubated at 30°C in the dark for 30 minutes before being pelleted again and washed in 500µl of YPD. They were then pelleted again and re-suspended in 1ml of YPD, before being transferred into a culture tube and incubated at 30°C in the dark in a rotary shaker for 30 min. Next, the cells were spun down and re-suspended in 30µl Phosphate Buffered Saline (PBS), ready to be visualised using the equipment described in *Section 2.3.1*. Cells were observed through an RFP filter set with an exposure time of 10ms.

2.3.2.2 Quinacrine staining of yeast vacuoles

Wild-type and *Δpor1* cells were grown in overnight cultures of 5ml SC media. The cells were washed three times in SC media buffered to pH of 7.5 with 50mM Na_2PO_4 buffer. The cell pellet was resuspended in 100µl of synthetic media + 2% glucose buffered to pH of 7.5 with 50mM Na_2PO_4 buffer with quinacrine (mwt 541.77) added to a final concentration of 200µM (from a 20mM stock made up in 50mM Na_2PO_4 buffer pH 7.5). The mixtures were incubated at 30°C for 20 minutes and

then were placed on ice. The cells were then washed three times in 500µl of ice-cold wash buffer (50mM Na_2PO_4 pH 7.5 + 2% glucose). The cells were pelleted at 8000 RPM for one minute and then re-suspended in 100µl of wash buffer and visualised using a GFP filter set on the equipment described in *Section 2.3.1* with an exposure time of 50ms.

2.3.2.3 LD540 staining of lipid droplets

Wild-type and *Δpor1* cells were grown in overnight cultures of 5ml YPD media. 200µl of overnight culture was then aliquoted into Eppendorf tubes and 0.2µl of 0.5mg/ml LD540 was added. The mixtures were left in the dark for 5 minutes and then pelleted at 8,000 RPM for 1 minute. The cells were then washed three times with media and resuspended in 50µl of sterile MilliQ water, ready to be visualised using the equipment described in *Section 2.3.1*. Cells were observed through an RFP filter with an exposure time of 10-25ms.

2.4 Western blotting

2.4.1 ATG8–GFP autophagy assay

Strains containing a low copy plasmid expressing ATG8–GFP were grown in SD-URA containing 2% glucose for 48 hours (to stationary phase). Following this, 1ml of culture at each timepoint (mid-log phase, 24 hours and 48 hours) was transferred to the same medium, lacking ammonium sulphate to induce autophagy via nitrogen starvation, and incubated at 30°C with 180 RPM shaking for 6 hours. Total protein was extracted from cells pre- and post-induction of autophagy and subjected to western blotting.

2.4.2 Whole cell protein extraction (all samples)

Cells were grown overnight in SD-URA media between mid-log phase and 48-hour growth as appropriate in a 30°C rotary shaker at 180 RPM, before protein samples were prepared by harvesting 1ml of overnight culture. The pelleted cells were then re-suspended in 200µl of lysis buffer (0.1 M NaOH, 0.05 M EDTA, 2% SDS, 2% β-mercaptoethanol). The samples were then heated for 10 minutes at 90°C before 5µl of 4M Acetic acid was added and the samples were vortexed for 30s. Following vortexing, a secondary incubation took place at 90°C for a further 10 minutes before

50µl of loading buffer (0.25 M Tris-HCl pH 6.8, 50% Glycerol, 0.05% Bromophenolblue) was added. To use the samples for western blotting, the lysate was cleared through centrifugation and the supernatant was loaded into an SDS PAGE (Sodium Dodecyl Sulfate–Polyacrylamide Gel Electrophoresis) gel.

2.4.3 Preparation of polyacrylamide gels.

All the samples were run on a 10% SDS PAGE gel composed of both a 5% stacking segment on top of a 12% resolving segment, the components of which can be seen in *Table 2-4*. The SDS PAGE gels were made up in a glass cassette (Biorad) 0.75mm thick. The first layer to be poured was the resolving layer, 6.5cm long from the bottom of the cassette. 1ml of isopropanol was added to ensure the resolving layer was separated from air, free from bubbles and level after the gel had been cast. After being left for 1 hour to set, the stacking segment was added up to the top of the cassette and a comb with 12 wells was placed into the top of the cassette. The gel was then left to set for a further hour.

Table 2-6: Components of the SDS PAGE gel.

Gel	***Component***	***Amount***
Stacking	0.5M Tris (pH 6.8) + 0.4% SDS	4 ml
	30% Acrylamide Mix	1.34 ml
	Tetramethylethylenediamine (TEMED)	8µl
	Sterile MilliQ water	4.572 ml
	10% APS (ammonium persulfate)	90µl
Resolving	1.5M Tris (pH 8.8) + 0.4% SDS	3.75 ml
	30% Acrylamide Mix	6 ml
	TEMED	6µl
	Sterile MilliQ water	6.156 ml
	10% APS	150µl

2.4.4 SDS-PAGE gel electrophoresis

The sample lysates from *Section 2.4.2* were taken and 10µl of each was loaded into the acrylamide gel and run for 90V for around 1 hour attached to a Biorad power supply, until the samples had passed through the stacking gel. The samples were then run at 110V for a further 2 hours until they had neared the bottom of the resolving gel. 5µl of Thermo Scientific PageRuler Plus Prestained Protein Ladder was used and 10µl of loading buffer was loaded into any empty wells.

2.4.5 Semi-dry protein transfer

The resulting separated proteins were transferred onto a Polyvinylidene Difluoride (PVDF) membrane through semidry transfer using a Biorad Trans SD machine. Four pieces of blotting paper of equal size to the resolving layer (4 x 9cm) were wetted in transfer buffer (50ml 10x transfer buffer (29g glycine, 58g Tris base, 40µl 10% SDS), 100ml methanol, 350ml MilliQ water) and the PVDF membrane (4x9cm) was wetted in methanol to activate it before being soaked in transfer buffer for 15 minutes. The transfer was layered with two pieces of blotting paper placed first followed by the PVDF membrane, the SDS PAGE gel, and finally two more pieces of blotting paper, ensuring all air bubbles were rolled out. The transfer was run at 25V for 30 minutes per gel.

2.4.6 Western blot detection using Enhanced Chemiluminescence (ECL)

After semi-dry transfer, the PVDF membrane was blocked in blocking buffer (5% semi skimmed milk powder, 1x PBS +0.2% Tween 20 (PBS/T)) for 45 minutes at room temperature on a rotary shaker. The membrane was then briefly rinsed in PBS/T and then placed in a 50ml Falcon tube with 5ml blocking solution with primary antibody at a dilution recommended by the manufacturer. The list of antibodies used for each gel can be seen in *Section 2.4.6*. The tube was left to incubate overnight at 4°C on a roller mixer. After overnight incubation, the membrane was removed and briefly washed in PBS/T twice before being washed for 15 min followed by two 5 min washes in PBS/T. The membrane was next placed in a 50ml Falcon tube with 5ml blocking buffer containing a horseradish conjugated secondary antibody at a dilution recommended by the manufacturer. The tube was left to incubate at room temperature for 30 min on a roller mixer.

After the incubation period was up the membrane was briefly washed twice in PBS/T twice before being washed for 15 min followed by three 5 min washes in PBS/T. The membrane was transferred to PBS. Two Electrochemiluminescence (ECL) solutions were made up as follows: Solution I (1 ml of 2.5 mM luminol, 440µl of 0.396 mM p-ccumaric acid, 10 ml of 1M Tris-HCL pH 8.5, 88.56ml of MilliQ sterile water). Solution II (64µl of 30% hydrogen peroxide, 10ml of 1M Tris-HCL pH 8.5, 89.94ml of MilliQ sterile water). The solutions were mixed at a 1:1 ratio and the membrane was drained of PBS. The mixed solutions were then poured on the membrane and left for exactly one minute before the excess was removed and the membrane was transferred to Saran wrap. The membrane in Saran wrap was transferred to a Syngene G: Box for imaging.

2.4.7 Antibodies used for protein detection

Primary antibody used for Slt2 detection: Rabbit Anti-Phosphpo-44/42 MAPK (Erk1/2) (Thr202/Tyr204) (Cell Signalling, catalogue number #4370) and was used at a dilution of 1/2000.

Primary antibody used for Porin detection: Mouse anti-VDAC1/Porin (Abcam, catalogue number # 16G9E6BC4) and was used at a dilution of 1/2000.

Primary antibody used for GFP detection: Mouse anti-GFP (Sigma, catalougue number 1181446000) used at a dilution of 1/1000.

Primary antibody used for actin detection: Sheep anti-actin, a kind gift from Prof. John Cooper (Washington University) and was used at a dilution of 1/2000.

Secondary antibody used for Slt2 detection: Anti-Rabbit IgG HRP (Sigma, catalogue number #A0545) and was used at a dilution of 1/5000.

Secondary antibody used for Porin and GFP detection: Anti-Mouse IgG HRP (Sigma, catalogue number #A4416) and was used at a dilution 1/5000.

Secondary antibody used for actin detection: Anti-goat IgG HRP (Sigma, catalogue number A3415) and was used at a dilution of 1/5000.

2.5 Flow Cytometry to detect PI as a marker of necrosis

2.5.1 Flow cytometry of cells in rich and selective media

Wild-type and *Δpor1* cells were grown overnight in YPD or SC media at 30°C on a rotatory shaker at 180 RPM, and then inoculated to an OD600 of 0.1 in a 48 well plate. The cultures were then incubated for a total of 168 hours at 30°C and shaken constantly. A mixture of 15ml of PBS and 60µl Potassium Iodide (PI) was made (PBS-PI) for cell suspension. At regular intervals of 24 hours, 30µl of cell culture was added to a Fluorescence-Activated Cell Sorter (FACS) tube along with 500µl PBS-PI. The mixtures were vortexed to allow thorough distribution of the cells throughout the buffer. A negative control contained 30µl cell culture and 500µl PBS with 0% PI. As a positive control, standard cells were treated with a 90°C heat shock for 10 min, and PI stained in the same way as the other samples. A total of 30,000 cells were analysed per sample using FACSCalibur with an FL-2 detector. A histogram plot was used to calculate the proportion of PI stained cells within the population. This experiment was repeated with cells that overexpress porin that were grown overnight in SD-URA media + glucose.

2.6 Standards for lipid quantification performed by Dr Patrick Rockenfeller (University of Graz) and Dr. Oskar Knittelfelder (Max Planck Institute of Molecular Cell Biology and Genetics (MPI-CBG) Dresden, Germany

Synthetic lipid standards were purchased from Avanti Polar Lipids, Inc. (Alabaster, USA). All used solvents were of at least High-Performance Liquid Chromatography (HPLC) grade. Stocks of internal standards were stored in glass ampoules at -20°C until used for the preparation of internal standard mix in 10:3 MTBE/MeOH. 700µl internal standard mix contained: 1778 pmol cholesterol d_7, 1040 pmol CE 16:0 d_7, 1000 pmol 50:0 TG d_5, 233 pmol 34:0 DG d_5, 1101 pmol 25:0 PC, 154 pmol LPC, 107 pmol 25:0 PS, 590 pmol 25:0 PE, 85 pmol 13:0 LPE, 384 pmol 25:0 PI, 109 pmol 25:0 PG, 73 pmol 30:1 Cer, 123 pmol 25:0 PA, 91 pmol 13:0 LPA, 32 pmol 13:0 LPI, 44 pmol 13:0 LPS, 75 pmol 13:0 LPG, 137 pmol 56:4 CL and 87 pmol 30:1 LacCer.

2.6.1 Lipid extraction and quantification by shotgun mass spectrometry

2 OD units of yeast were homogenized with 0.5mm zirconia beads in a cooled tissuelyzer for 2 x 10 min at 30Hz in 300µl IPA. The whole homogenate was evaporated in a vacuum desiccator to complete dryness. Lipid extraction was performed according to[106-108]. In brief, 700µl internal standard mix in 10:3 MTBE/MeOH was added to each sample and vortexed for 1h at 4°C. After addition of 140µl H_2O samples were vortexed for another 15 min. Phase separation was induced by centrifugation at 13400 rpm for 15 min. The organic phase was transferred to a glass vial and evaporated. Samples were reconstituted in 300µl 1:2 MeOH/$CHCl_3$. For lipidome 5µl of sample were diluted with 95µl 4:2:1 IPA/MeOH/CHCl3 + 7.5 mM ammonium formate.

Mass spectrometric analysis was performed on a Q Exactive instrument (Thermo Fischer Scientific, Bremen, DE) equipped with a robotic nanoflow ion source TriVersa NanoMate (Advion BioSciences, Ithaca, USA) using nanoelectrospray chips with a diameter of 4.1 um. The ion source was controlled by the Chipsoft 8.3.1 software (Advion BioSciences). Ionization voltage was + 0.96 kV in positive and − 0.96 kV in negative mode; back pressure was set at 1.25 psi in both modes. Samples were analyzed by polarity switching[108]. The temperature of the ion transfer capillary was 200 °C; S-lens RF level was set to 50%. Each sample was analyzed for 18 min. FT-MS spectra were acquired within the range of m/z 400–1000 from 0 min to 0.2 min in positive and within the range of m/z 350–1200 from 6.2 min to 6.4 min in negative mode at a mass resolution of R m/z 200 = 140000, automated gain control (AGC) of 3 x 10^6 and with an maximal injection time of 3000 ms. Ergosterol was determined by parallel reaction monitoring (PRM) FT-MS/MS between 0.2 to 1.7 min. For FT-MS/MS micro scans were set to 1, isolation window to 0.8 Da, normalized collision energy to 12.5%, AGC to 5 × 10^4 and maximum injection time to 3000 ms. t-SIM in positive (1.7 to 6 min) and negative (6.4 to 18 min) mode was acquired with R m/z 200 = 140000; automated gain control of 5 × 10^4; maximum injection time of 650 ms; isolation window of 20 Th and scan range of m/z 400 to 1000 in positive and m/z 350 to 1200 in negative mode, respectively. The inclusion list of masses targeted in t-SIM analyses started at m/z 355 in negative and m/z 405 in positive ion mode and other masses were computed by adding 10 Th increment (i.e. m/z 355, 365, 375, …) up to m/z 1005

in positive mode and up to m/z 1205 in negative mode. All acquired spectra were filtered by PeakStrainer (https://git.mpi-cbg.de/labShevchenko/PeakStrainer/wikis/home)[109] and stitched together by an in-house developed script[110]. Lipids were identified by LipidXplorer software[111]. Molecular Fragmentation Query Language (MFQL) queries were compiled for ergosterol, ergosterol esters, PC, LPC, PE, LPE, PI, LPI, Cer, IPC, MIPC, $M(IP)_2C$, PA, LPA, PG, LPG, PS, LPS, TG, and DG lipid classes. The identification relied on accurately determined intact lipid masses (mass accuracy better than 5 ppm) and signal to noise threshold higher than 3. Lipids were quantified by comparing the isotopically corrected abundances of their molecular ions with the abundances of internal standards of the same lipid class. Complex sphingolipids (IPC, MIPC, $M(IP)_2C$) were normalized to 30:1 LacCer and ergosterol as well as ergosterol esters were normalized to cholesterol and to CE, respectively.

3. Results

3.1 Loss of POR1 leads to a change in mitochondrial morphology

We wished to determine whether loss of POR1 led to changes in mitochondrial morphology. To achieve this, we introduced a plasmid that expresses a mitochondrial targeted GFP into *Δpor1* cells and compared mitochondrial distribution to wild type using fluorescence microscopy. Images were taken in both log phase (*Figure 3-1 a, b*) and stationary phase (*Figure 3-1 c, d*) Interestingly, porin null cells (*Figure 3-1b*) did not display observable morphological differences to wild type during log phase growth (*Figure 3-1a*). However, in stationary phase a proportion of *Δpor1* cells displayed an aggregated mitochondrial morphology, forming large, ectopic clumps. At this stage, 2.3% of wild-type cells showed mitochondrial aggregation (*Figure 3-1c*) in comparison to 28.4% of *Δpor1* cells (*Figure 3-1d)*. These data suggest that loss of POR1 does not affect inheritance of mitochondria during log phase but points to a defect in morphology during post-diauxic shift when both mitochondrial biogenesis and oxidative phosphorylation increase in cultures supplemented with glucose.

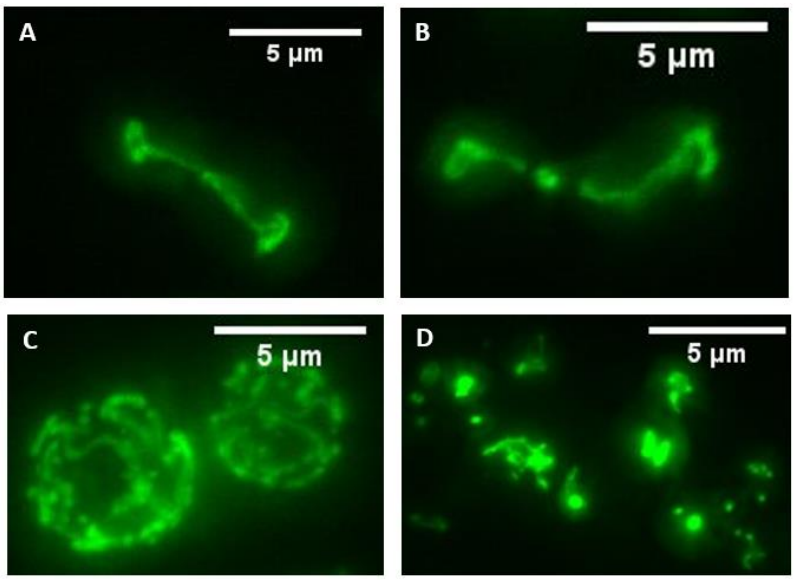


Figure 3-1: The mitochondrial morphology of wild-type and Δpor1 cells.

Wild-type (**A, C**) and *Δpor1* (**B, D**) cells containing a mitochondrial-GFP plasmid were grown in selective media and visualised during log phase (**A, B**) and stationary phase (**C, D**). *Δpor1* cells mirrored the wild type during log phase but show a clumped phenotype in stationary phase cells (**D**).

3.2 Loss of porin leads to a loss of respiration

Given the role that porin plays in movement of molecules in and out of the mitochondria and in response to the morphological defects observed in *Section 3.1*, respirometry assays were carried out on both wild-type and *Δpor1* cells during stationary phase. The cells were analysed after 24-hour growth in selective media (SD-URA) containing either 2% glucose (*Figure 3-2a*) or 2% glycerol (*Figure 3-2b*) as carbon sources. Interestingly, the results indicate that *Δpor1* cells are unable to respire during stationary phase, regardless of the carbon source that they are grown in (*Figure 3-2).* This was done by adding 50mM TET, which inhibits ATP synthase to determine LEAK respiration, 12mM FCCP, an ionophore that uncouples the electron transport chain from the oxidative phosphorylation system, and 20mM of Antimycin A, which determined non-mitochondrial respiration. *Δpor1* cells only show non-mitochondrial respiration regardless of the drugs added.

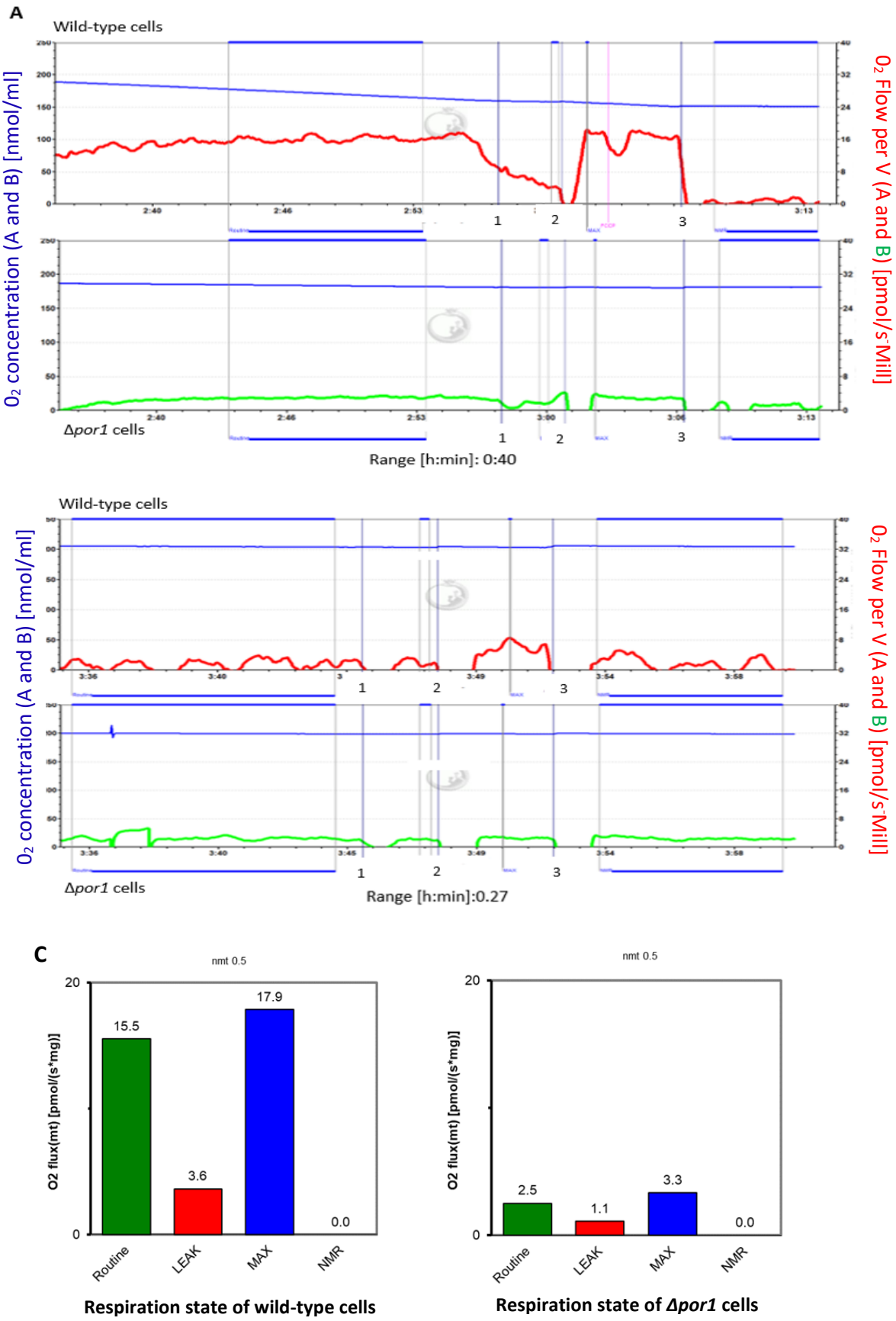


Figure 3-2: Respirometry assays of wild-type and Δpor1 cells during stationary phase.
Respirometry assays of overnight cultures of wild-type (**red**) and *Δpor1* (**green**) cells grown in either glucose (**A**) or glycerol (**B**). Triethyltin Bromide (TET), FCCP and Antimycin A (AntA) was added to each chamber at point 1, 2 and 3, respectively, and the resultant ROUTINE, LEAK (TET), MAX (FCCP) and NMR (AntA) values were recorded, as shown in (**C**). Mitochondria of *Δpor1* exhibited low respiration in comparison to wild-type cells. LEAK = (proton) leak respiration, ROUTINE = routine respiration before any drugs added, MAX = maximum respiration, NMR = Non—Mitochondrial Respiration.

3.3 Growth patterns of wild-type and Δpor1 cells

3.3.1 Loss of porin stunts cellular growth

In order to assess how the respiratory phenotype shown in *Section 3.2* affected cellular growth, growth assays of wild-type and *Δpor1* strains were carried out in YP (*Figure 3-3*) or selective media (SC) (*Figure 3-4*) using either glucose or glycerol as carbon sources, whereby readings were taken every six minutes. In YP media, wild-type cells reached a higher final OD when compared to *Δpor1* cells when supplemented with either glucose or glycerol (*Figure 3-3*). However, growth of *Δpor1* cells was very poor in glycerol containing media. As functional mitochondria are required for the metabolism of glycerol, a non-fermentable carbon source, these data also indicate a reduction in in the ability to respire. The differences in growth between wild-type and Δ*por1* cells are reflected in the exponential growth rates, whereby the growth rate constant (μ) is equal to the change in OD per hour. For growth in YP media, the average growth rate constant for wild-type cells was 0.308μ and 0.305μ for a glucose carbon source and 0.122μ and 0.131μ for a glycerol carbon source. Δ*por1* cells had growth rate constants of 0.220μ and 0.239μ when grown with glucose but did not enter into exponential growth when grown in glycerol.

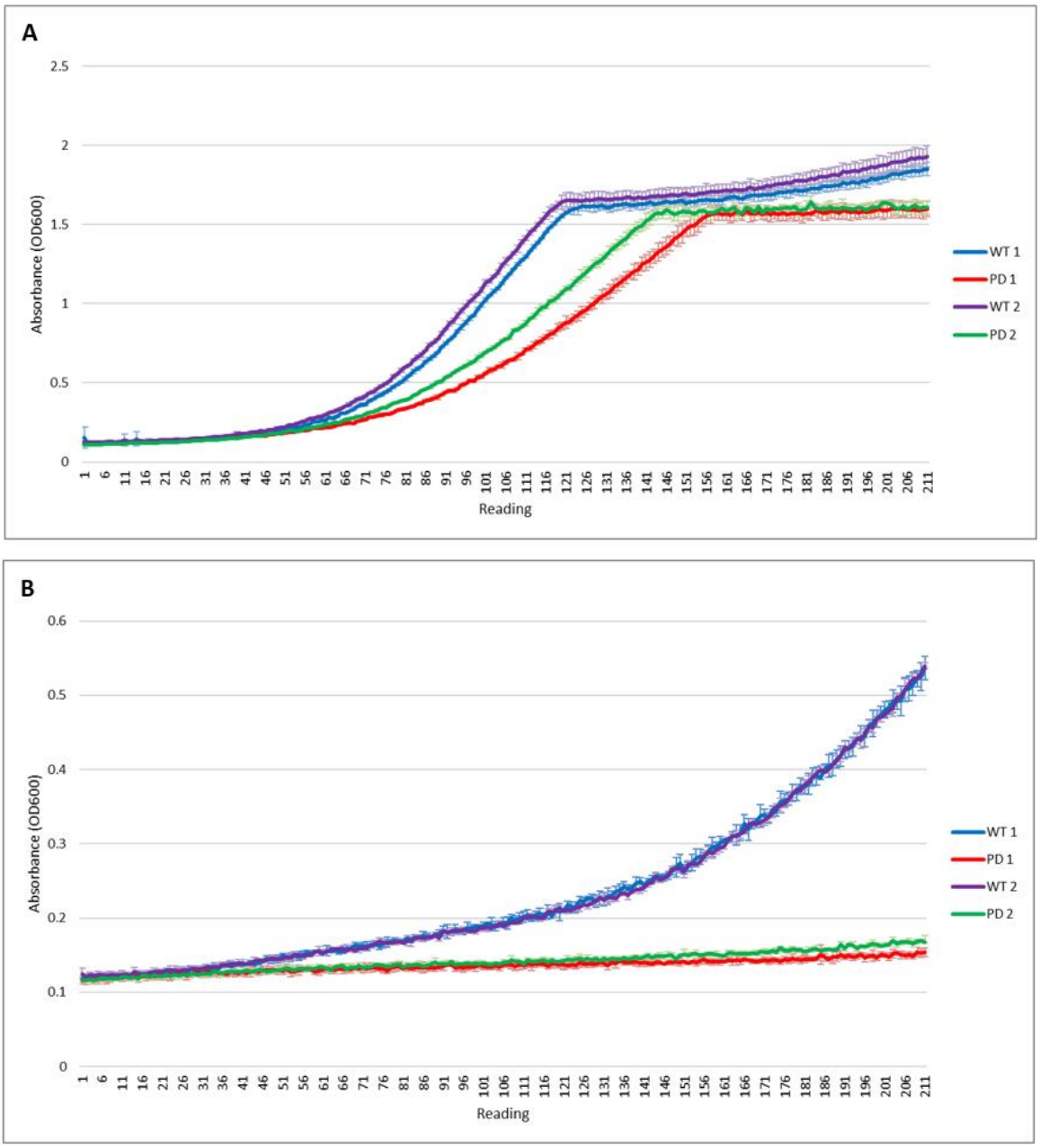


Figure 3-3: Growth assays of wild-type and Δpor1 cells grown in YP media.
Wild-type (WT) and *Δpor1* cells (PD) were grown in YP media containing either glucose (**A**) or glycerol (**B**) and absorbance values (OD600) were taken at 6-minute intervals up to 211 readings. Cells lacking porin have a lower absorbance reading than the wild type regardless of carbon source. Error bars based on standard deviation which was calculated from triplicate values (n=3). μ = change in OD / hour.

The growth rate constants for cells grown in SC media were similar to the values for cells grown in YP media. Wild-type cells had growth rate constant values of 0.265μ and 0.264μ in glucose and 0.075μ and 0.073μ in glycerol, respectively. Δ*por1* cells, however, had values of 0.238μ and 0.245μ when grown in SC media with glucose and 0.066μ when grown in glycerol. These growth rates are plotted in *Figure 3-5.*

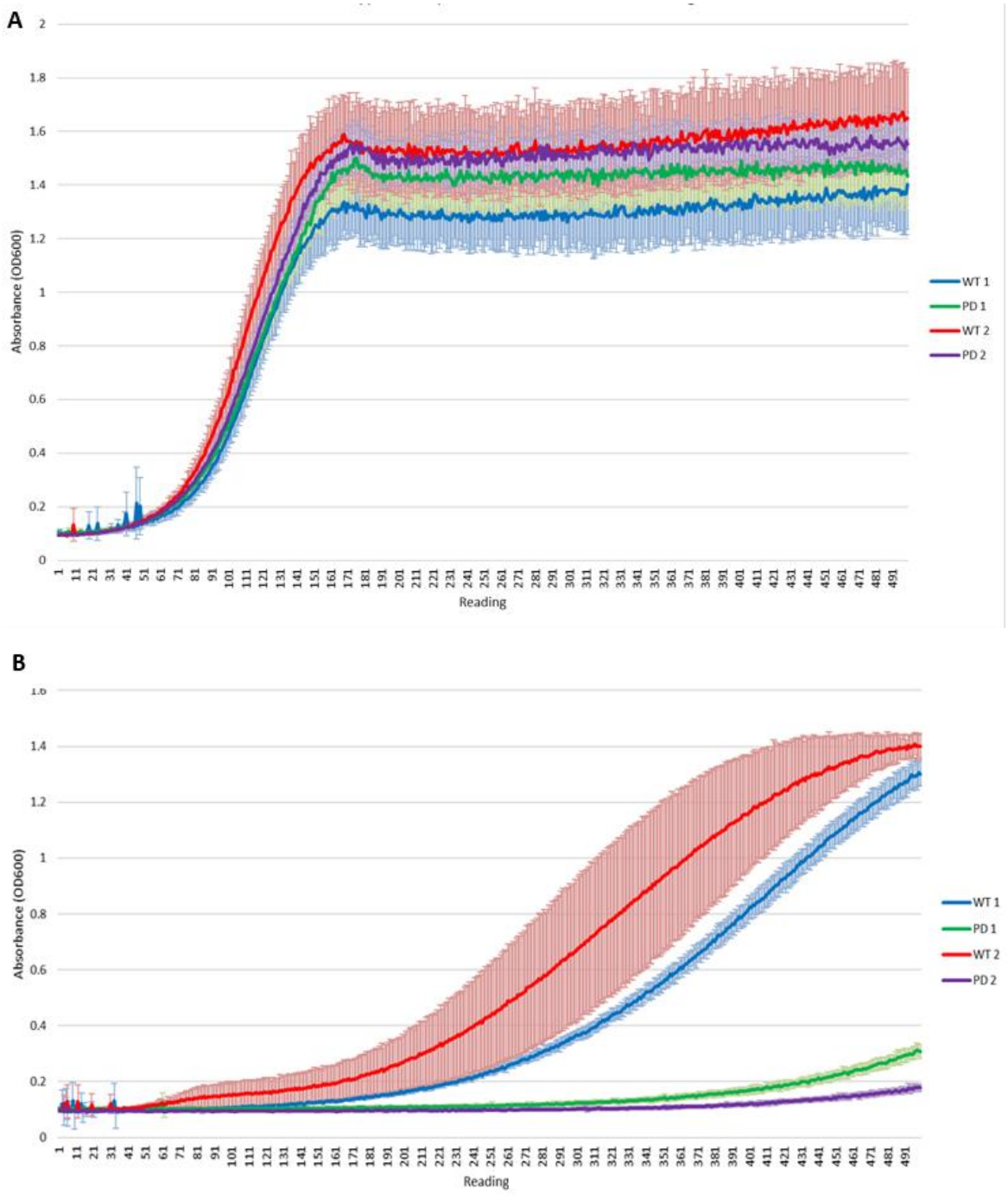


Figure 3-4: Growth assays of wild-type and Δpor1 cells grown in selective media.
Wild-type (WT) and *Δpor1* cells (PD) were grown in selective media (SC) containing either glucose (**A**) or glycerol (**B**) and absorbance values (OD600) were taken at 6-minute intervals up to 491 readings. Cells lacking porin display stunted growth in both cases. Error bars based on standard deviation which was calculated from triplicate values (n=3). μ = change in OD / hour.

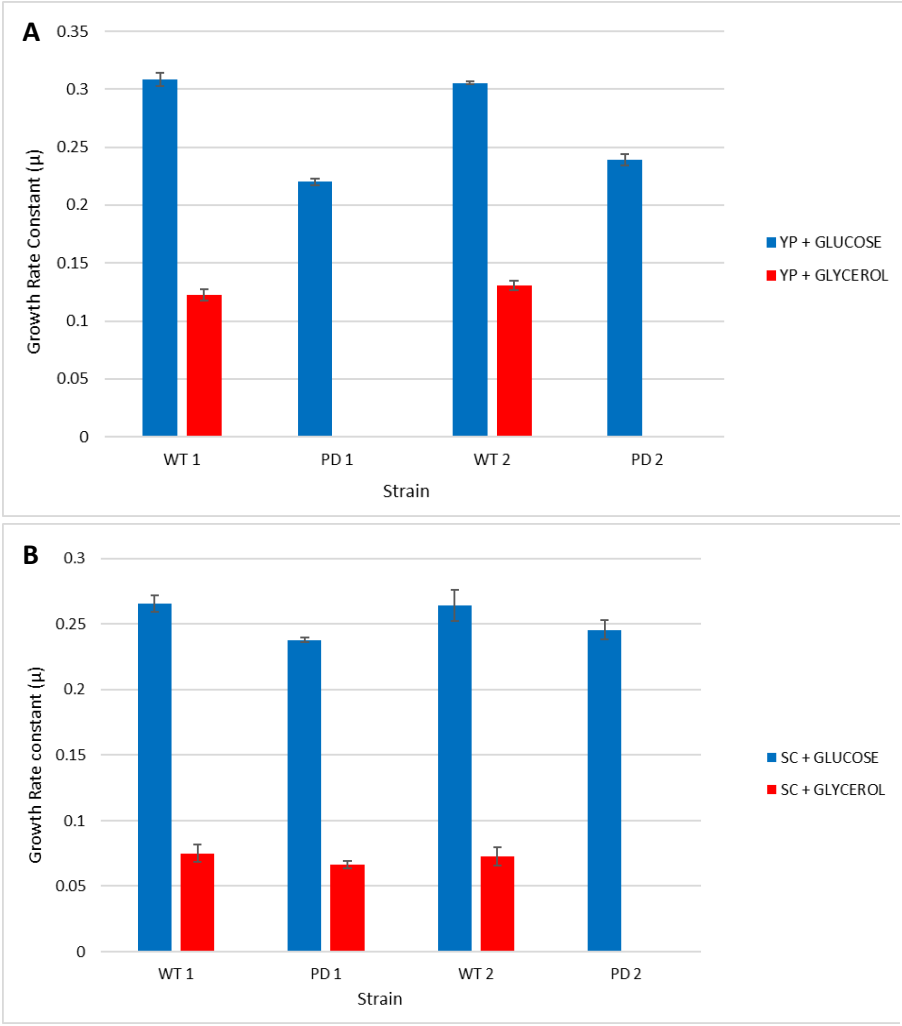


Figure 3-5: Summary of the exponential growth rates of wild-type and Δpor1 cells. Exponential growth rate of wild-type and *Δpor1* cells in ***(A)*** YP media and (**B**) SC media. (**A**) No values for glycerol grown *Δpor1* cells are given as the cells did not enter exponential growth (log phase). Growth rate constants (μ) were calculated from data given in growth assays (*Figure 3-3* and *3-4*). In both cases, the growth rate of *Δpor1* cells is lower than that of the wild type. Error bars based on standard deviation which was calculated from triplicate values (n=3). μ = change in OD / hour.

These results show that a loss of porin reduces cellular growth regardless of media or carbon source, although Δ*por1* cells have a lower growth rate in rich media compared to selective media – which suggests that porin may play a role in nutrient intake. However, while glucose is the preferred carbon source for both strains, wild-type cells can utilise glycerol for growth in selective media more than in rich media (YP), which is reflected by the absorbance values in *Figures 3-3* and *3-4*. The lack of growth displayed by *Δpor1* cells in glycerol indicates that unlike the wild type, these cells cannot utilise glycerol efficiently as they are unable to respire, which is a necessary step for the metabolism of glycerol.

3.3.2 The growth defect displayed by Δpor1 cells can be rescued by re-expression of POR1

To clarify whether the growth defect observed in *Δpor1* cells in *Section 3.3.1* could be rescued, growth assays of both wild-type and *Δpor1* cells containing a plasmid that expressed POR1 from a

GPD promoter (PCG633) and an empty vector plasmid (PCG557) was conducted. These strains were grown in selective media (SD-URA) with either glucose (*Figure 3-6A*) or glycerol (*Figure 3-6B*) as carbon sources.

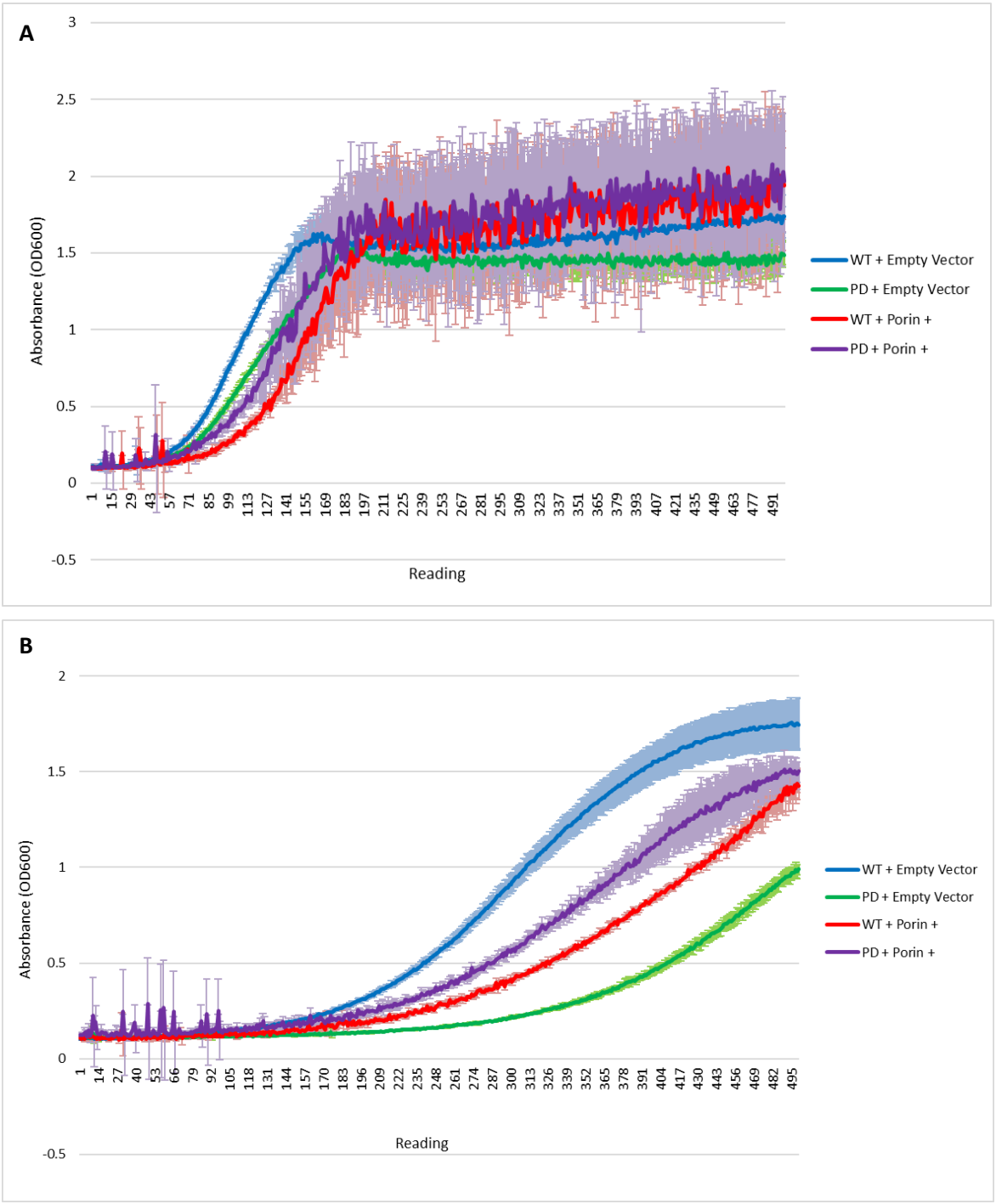


Figure 3-6: Growth assays of porin overexpression strains in selective media.
Samples of wild-type (WT) and *Δpor1* (PD) cells containing a porin overexpression plasmid (Porin +) and a control plasmid (Empty Vector) were grown in selective media (SD-URA) containing either glucose (**A**) or glycerol (**B**). Absorbance values (OD600) were taken at 6-minute intervals up to 495 readings. In both cases, porin overexpression rescues the stunted growth phenotype of *Δpor1* cells. Error bars based on standard deviation which was calculated from triplicate values (n=3). μ = change in OD / hour.

During stationary phase, there is no increase in OD in *Δpor1* cells in grown in glucose due to a lack of respiration. For cells grown with a glucose carbon source in log phase, the growth rate constant of wild-type and Δ*por1* cells containing an empty plasmid was 0.066µ and 0.068µ, respectively (*Figure 3-7*). When grown in media containing glycerol, wild-type cells transformed with an empty vector plasmid had a growth constant of 0.108µ and Δ*por1* cells transformed with an empty vector plasmid had a value of 0.082µ. Wild-type and Δ*por1* cells containing a porin re-expression plasmid had growth rate constants of 0.214µ and 0.173µ when grown in glucose, and 0.077µ and 0.082µ when grown in glycerol, respectively (*Figure 3-7*). Interestingly, when cells containing the empty vector plasmid are grown in glycerol, the growth rate constant is higher than the values for glucose. However, *Figure 3-6b* confirms that these cells enter exponential growth later than cells that re-express POR1. The growth rate constant for both wild-type and Δ*por1* cells containing a porin re-expression plasmid is similar to that of wild-type cells seen in *Figure 3-3* and *3-4*.

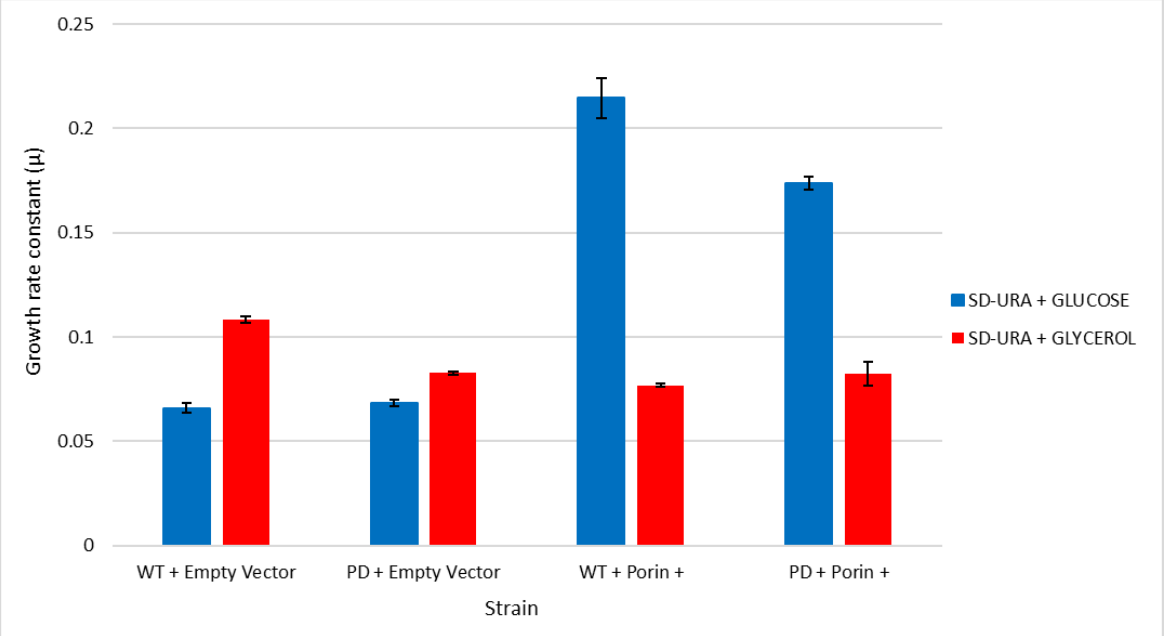


Figure 3-7: Summary of the exponential growth rates of wild-type and Δpor1 cells.
Exponential growth rates of wild-type (WT) and *Δpor1* cells (PD) with either an empty vector plasmid (Empty Vector) or a porin re-expression plasmid (Porin +) in SD-URA. Growth rate constants (µ) were calculated from data given in growth assays (*Figure 3-6*). Error bars based on standard deviation which was calculated from triplicate values (n=3). µ = change in OD / hour.

These data show that the poor growth phenotype displayed by *Δpor1* cells in *Section 3.3.1* is rescued in POR1 re-expression cells, which highlights, along with *Section 3.2,* that a loss of porin is responsible for loss of respiratory function, which impacts on cellular growth. While these data

show that re-expression of porin leads to a significant improvement in growth when compared to loss of porin, both wild type and porin expression strains grow less well than the wild type. This suggests that while re-introducing porin recovers growth to some extent, both loss and an increase in porin leads to cellular fitness defects.

3.4 Autophagy in wild-type and Δpor1 cells

3.4.1 Cells lacking porin exhibit reduced levels of autophagy

Following observation of dysfunctional mitochondria in porin null mutants, autophagy levels were monitored in order to assess how the cells were responding to the respiratory defect. Firstly, wild-type and *Δpor1* cells were transformed with an ATG8-GFP plasmid, which can be used to monitor the process of autophagy and the formation of autophagosomes and was observed using fluorescence microscopy over 48 hours (*Figure 3-8)*. Both strains were grown in SD-URA before transfer to nitrogen starvation media to induce autophagy as a positive control. The levels of cytosolic ATG8-GFP foci and the percentage of vacuoles with free GFP, generated during uptake of GFP into the vacuole after autophagosome fusion, were calculated. When the cells undergo autophagy, ATG8-GFP is cleaved upon vacuolar fusion with the ATG8 as part of the autophagosomal membrane, leaving free GFP in the vacuole. In log phase cells, there was little difference between strains whereby 10% of wild-type cells showed cytosolic ATG8-GFP foci in SD-URA media (*Figure 3-8a*) and 11.7% of cells showed ATG8-GFP foci in nitrogen starvation media (*Figure 3-8b*). For *Δpor1* cells, 12% and 13.8% of cells showed ATG8-GFP foci in SD-URA (*Figure 3-8c*) and nitrogen starvation media (*Figure 3-8d*), respectively.

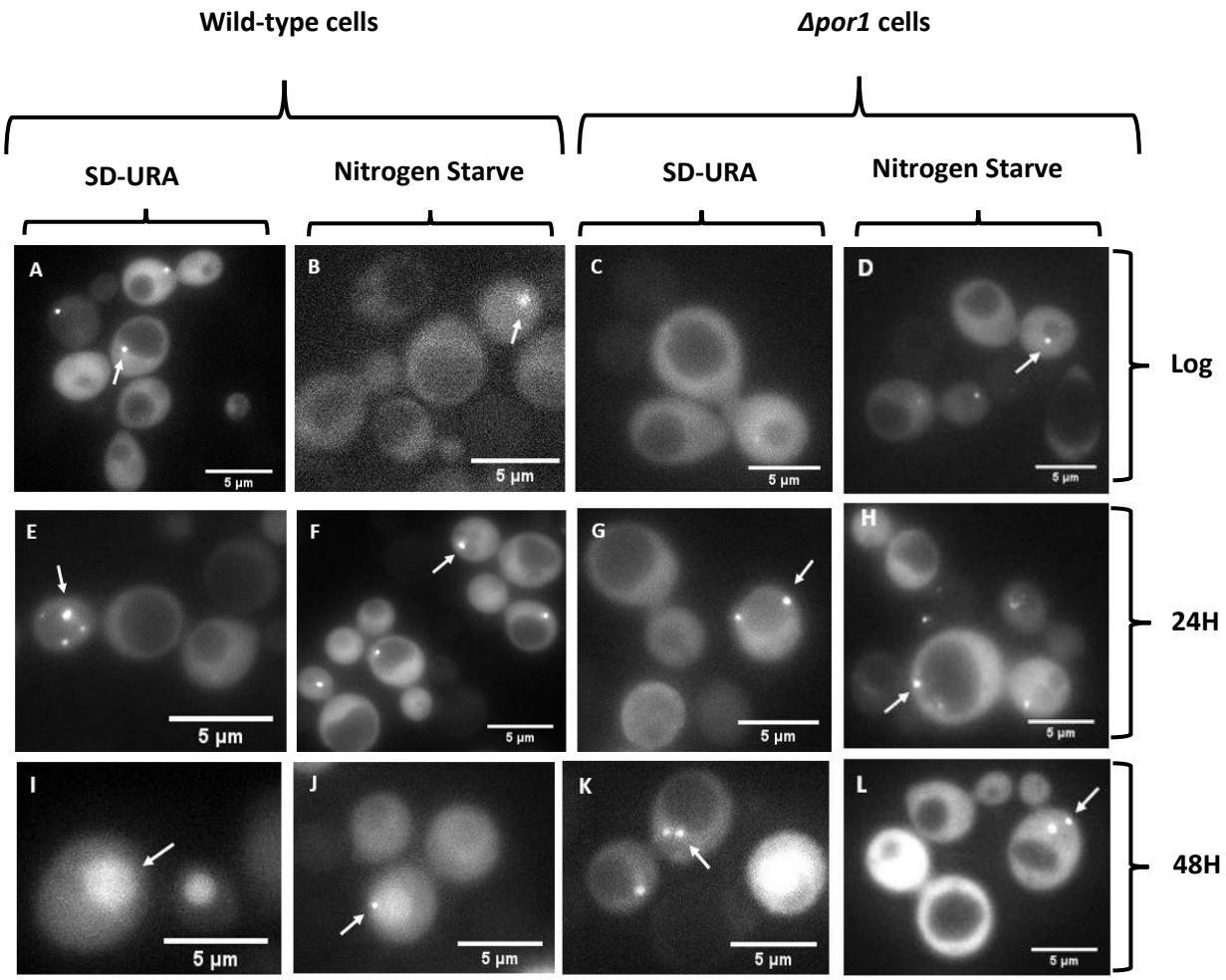


Figure 3-8: Observation of autophagy efficiency in wild-type and Δpor1 cells.
Wild-type (WT) and Δ*por1* cells were transformed with an ATG8-GFP plasmid and observed over 48 hours after growth in SD-URA and transfer to nitrogen starvation media (nitrogen starve). **A-D**) log phase growth (Log) where (**A**) is wild-type cells in SD-URA and (**B**) in nitrogen starvation media. **C**) *Δpor1* cells in SD-URA and (**D**) nitrogen starvation media. (**E-H**) 24-hour growth (24H) of wild-type (**E**) and *Δpor1* cells (**G**) in SD-URA and in nitrogen starvation media (**F** and **H**, respectively). **I-L**) 48-hour growth (48H) of wild-type cells in SD-URA (**I**) and nitrogen starve media (**J**) and *Δpor1* cells in both SD-URA (**K**) and nitrogen starvation media (**L**). Both ATG8-GFP foci and free vacuolar GFP are shown by arrows.

After 24 hours of growth, shown in *Figure 3-8e* to *3-8h*, 18.4% of wild-type cells showed cytosolic ATG8-GFP foci and 4.6% of cells showed free vacuolar GFP in SD-URA. After growth in nitrogen starvation media, 24% of cells showed ATG8-GFP foci in the cytosol and 1.2% of cells showed free GFP in the vacuole. 8.8% of *Δpor1* cells, on the other hand, showed cytosolic ATG8-GFP foci and 2.6% showed free vacuolar GFP. After 48 hours of growth in both SD-URA and nitrogen starvation media, shown in *Figure 3-8i* to 3.8*l*, a greater shift to free GFP was observed by wild-type cells in both cases, with 0.9% of cells showing cytosolic ATG8-GFP foci and 26.9% of cells showing free GFP in SD-URA. In nitrogen starvation media, ATG8-GFP foci were seen in 6% of wild-type cells and free

vacuolar GFP was seen in 11.4% of cells. Because there was no calculated increase in ATG8-GFP foci or GFP filled vacuoles in cells after transfer to nitrogen starvation media, this indicates that the positive control failed and should be repeated in future experiments for active autophagy induction.

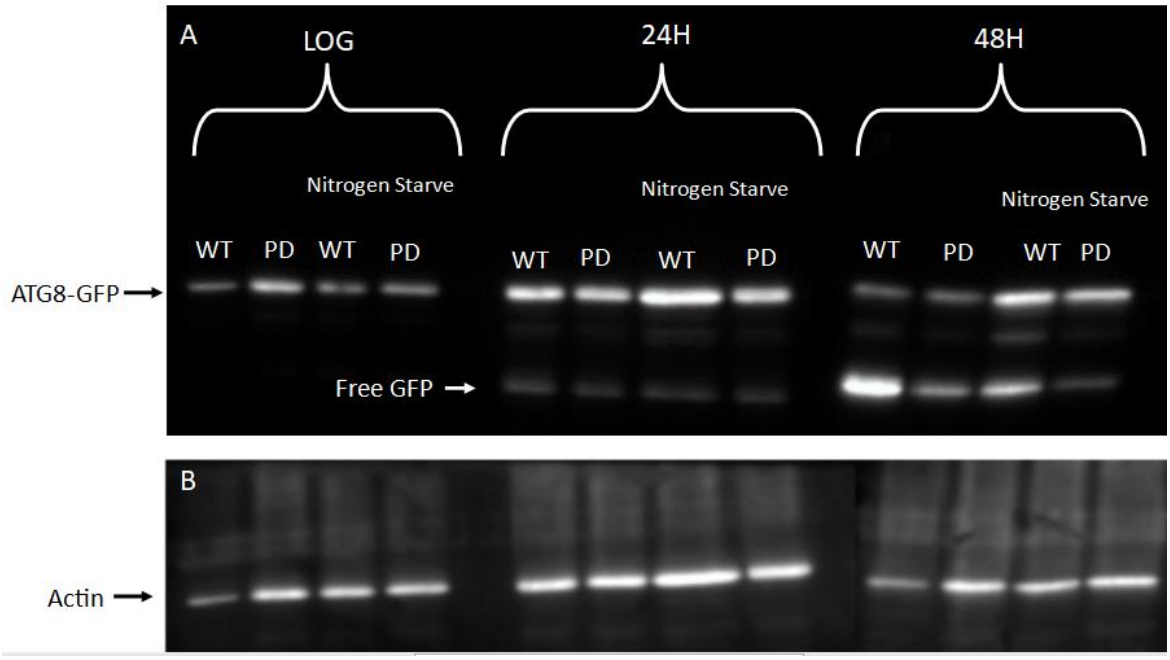


Figure 3-9: Western blot showing the levels of ATG8-GFP in both wild-type and Δpor1 cells.
A) Samples of both wild-type (WT) and Δ*por1* cells (PD) from visualisation were taken at log phase (LOG), 24 hours (24H) and 48 hours (48H) to detect the levels of ATG8-GFP and free (cleaved) GFP at each stage. Cells were also placed in nitrogen starvation media (Nitrogen Starve) as a positive control. Wild-type cells, particularly at 48 hours, display a much higher level of free vacuolar GFP, indicating that there is an autophagy defect in *Δpor1* cells. **B**) Actin loading control displaying the levels of loaded protein.

While these images gave some indication that Δ*por1* cells may have an autophagy defect, a western blot of extracted ATG8-GFP was carried out in order to quantify the levels of protein present at each stage, which is shown in *Figure 3-9*.

Interestingly, these data indicate that there is an autophagy defect in *Δpor1* cells, rather than an expected increase, as the gel shows fainter and thinner bands for both the ATG8-GFP foci and the free GFP in Δ*por1* cells in comparison to the wild type. In this case, the displayed defect could be due to either a change in the autophagic pathway or a lack of vacuolar integrity.

3.4.2 Vacuole morphology and acidification are not affected by the loss of POR1.

Considering the data from *Section 3.4.1*, which highlights that there is an autophagy defect in Δ*por1* cells, vacuolar staining was carried out to determine both the vacuole morphology and acidification in wild-type and Δ*por1* cells. This is because a change in vacuolar morphology, or fragmentation, may have accounted for the autophagy defect. Wild-type and *Δpor1* cells were grown to stationary phase and stained with FM4-64 as per *Section 2.3.2.1* (*Figure 3-10*) in order to assess the vacuolar structure of both strains following 24 hours and 48 hours of growth.

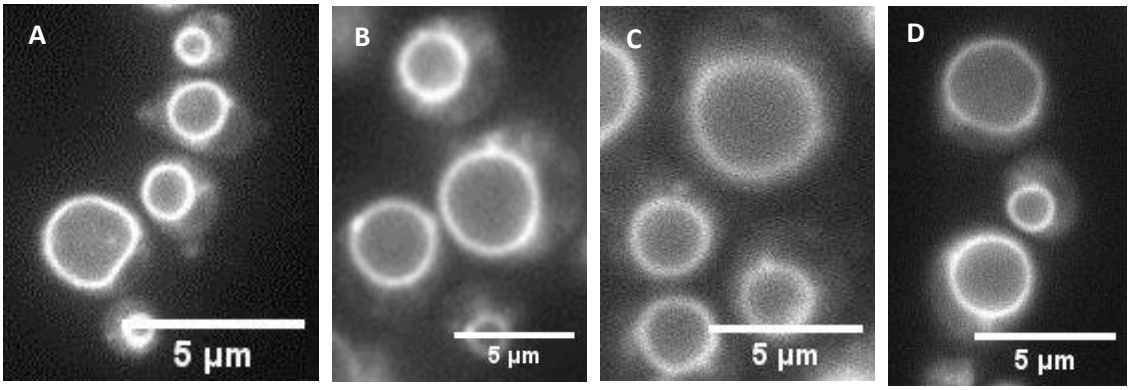


Figure 3-10: Vacuole structure of wild-type and Δpor1 cells.

Wild-type (**A, C**) and *Δpor1* (**B, D**) cells were stained with FM4-64 dye to observe vacuolar structure over 24 hours (**A, B**) and 48 hours (**C, D**). Both strains showed intact vacuoles at both stages.

Because *Δpor1* cells possessed a wild type vacuolar morphology, strains were stained with Quinacrine in order to observe the acidification of this compartment. The cells were stained after 24 hours (shown in *Figure 3-11)* whereby Δ*por1* cells mirrored the wild type in vacuole acidification.

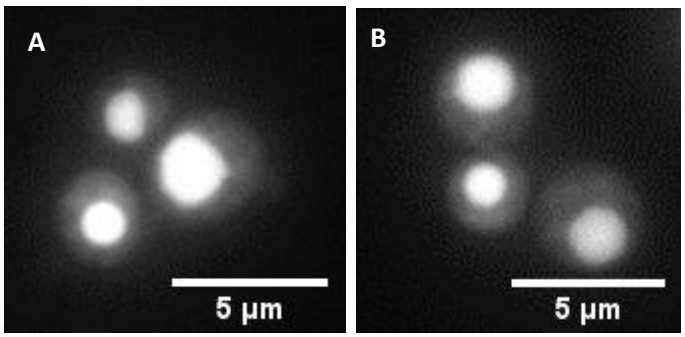


Figure 3-11: Vacuole acidity of wild-type and Δpor1 cells.

Wild-type (**A**) and *Δpor1* (**B**) cells were stained with Quinacrine after 24 hours to assess whether the vacuoles were acidified.

These data suggest that the vacuolar morphology and function of *S. cerevisiae* cells is not affected by a loss of POR1. This may suggest that the autophagy defect displayed by *Δpor1* cells is not attributable to loss of vacuole integrity.

3.5 Lipidomics of wild-type and Δpor1 cells

3.5.1 Δpor1 cells exhibit a different composition of lipids in their cell wall

Given that mitochondrial function is important for the coordination of lipid biosynthesis we sought to examine the effects of loss of POR1 upon the distribution of lipid species in Δ*por1* cells. In order to investigate the autophagic pathway of *Δpor1* cells, lipidomic studies were carried out in collaboration with Dr Patrick Rockenfeller (University of Graz) and Dr. Oskar Knittelfelder (Max Planck Institute of Molecular Cell Biology and Genetics (MPI-CBG) Dresden, Germany. The lipidomic profiles assessed showed a significant increase in Phosphatidylcholine (PC), Phosphatidylserine (PS), and Ceramide (Cer) levels in *Δpor1* cells when compared to wild type (*Figure 3-12*). In contrast, a decrease of Phosphatidylethanolamine (PE), Cardiolipin (CL) and Diacylglycerol (DG) was observed in *Δpor1* cells when compared to wild type.

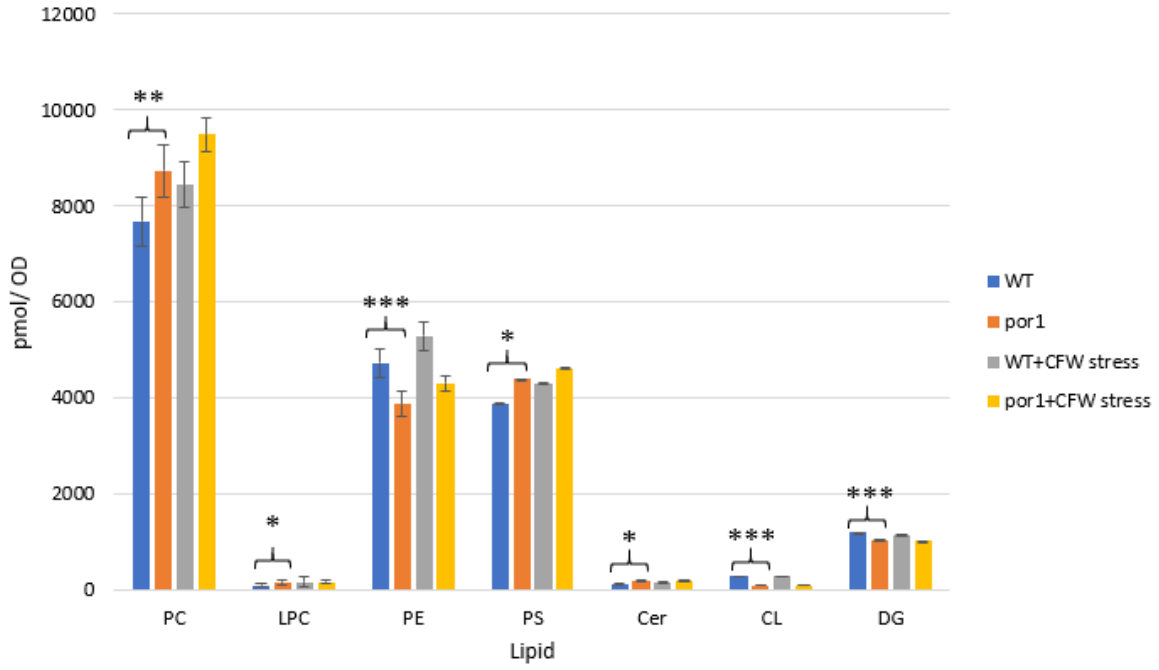


Figure 3-12: Lipid Composition of the cell wall of S. cerevisiae.
Lipidomic profile showing the cell wall lipid composition of *S. cerevisiae* cells. Wild-type (WT) and *Δpor1* (PD) lipid levels were compared against a calcofluor white stress as a positive control (CFW stress). PC = Phosphatidylcholine, LPC = Lysophosphatidylcholine, PE = Phosphatidylethanolamine, PS = Phosphatidylserine, Cer = Ceramide, CL = Cardiolipin, DG = Diacylglycerol. Error bars are based on standard deviation where (n=7). P(T<=t) values were based on comparison of the wild-type and *Δpor1* cells for each lipid shown. *0.01< P(T<=t) <0.05, **0.005< P(T<=t) <0.01, ***P(T<=t) <0.005.

Changes in lipid contributions may lead to alterations in the cell wall architecture. To examine this, Transmission Electron Microscopy (TEM) following High Pressure Freezing and Embedding (HPFE) of wild-type and Δ*por1* cells was carried out. Preparation of samples and imaging was carried out in collaboration with Dr. Dagmar Kolb-Lenz (Center for Medical Research, Core Facility Ultrastructure Analysis, University of Graz). To assess inner and outer cell wall thickness, 20 measurements were taken from each cell using a measuring tool in image J (10 for each wall) from multiple cells (7 wild type, 9 Δ*por1* cells) to obtain an average thickness (*Figure 3-13*). This data suggests that both the inner and outer wall of *Δpor1* cells is significantly thinner than wild type.

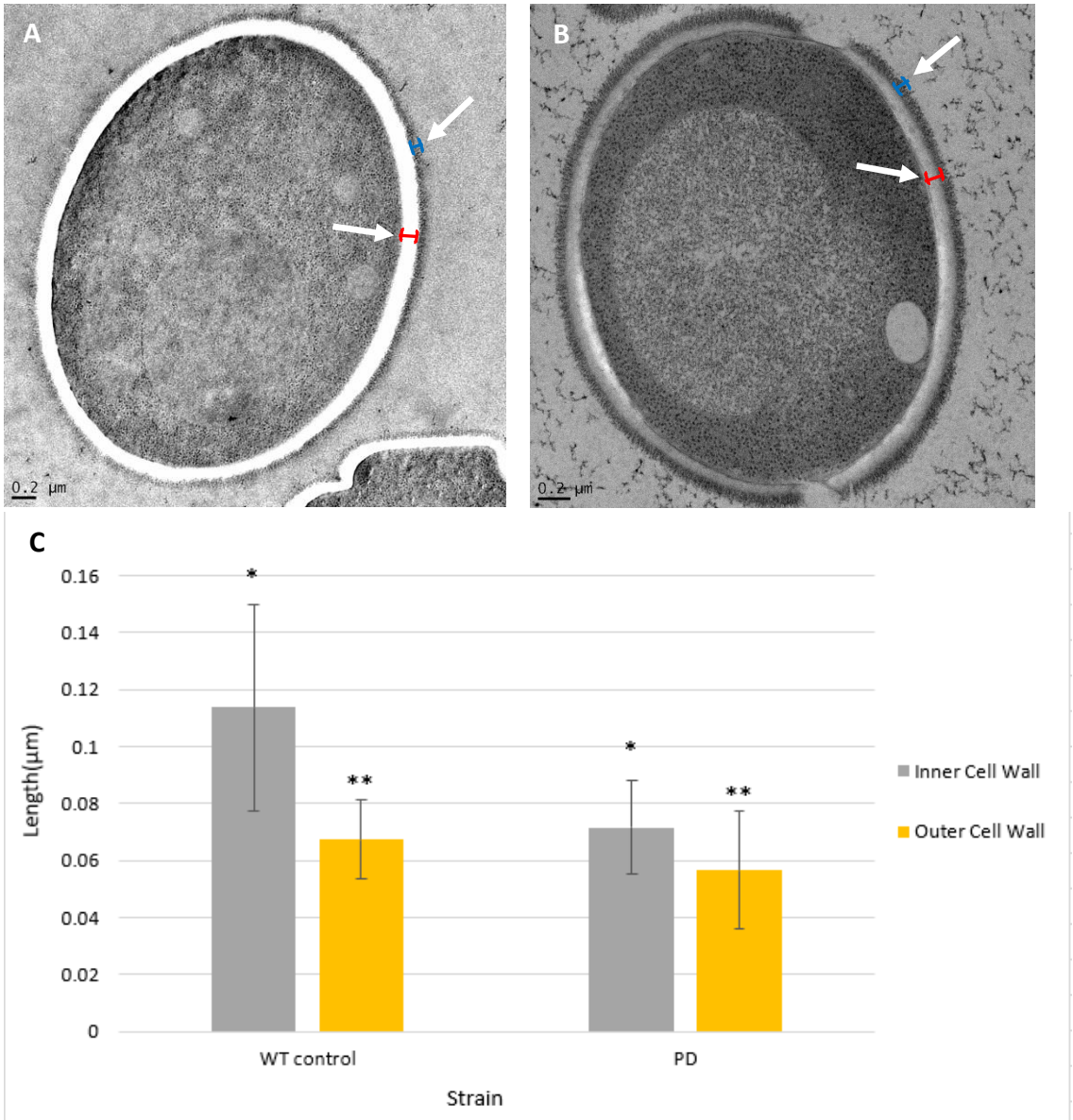


Figure 3-13: Cell wall thickness of wild-type and Δpor1 cells.
A) Measurements of both the inner membrane (white) and outer membrane (black) were taken from wild-type (WT) and **B**) *Δpor1* cells (PD). The measurements were taken using the image J measuring tool and examples are represented by red lines for the inner cell wall and blue lines for the outer cell wall. Images provided by Dr. Dagmar Kolb-Lenz. **C**) This data shows that both the inner and outer cell walls are significantly thinner in *Δpor1* cells. Error bars based on standard deviation where wild-type (n=7) and *Δpor1 (*n=9). *P(T<=t) 0.013, **P(T<=t) 0.033.

This data confirms that loss of POR1 leads to changes in both lipid homeostasis and cell wall structure. To assess whether changes in lipid biosynthesis led to changes in lipid storage, wild-type and *Δpor1* cells were stained with LD540 to visualise lipid droplet number in stationary phase cells (*Figure 3-14*). After 24 hours, 56.5% of wild-type cells had 4 or more lipid droplets (*Figure 3-14a*) and 61.5% *Δpor1* cells had more than 4 lipid droplets per cell (*Figure 3-14b*). After 48 hours, 87.2% of wild-type cells had more than 4 lipid droplets (*Figure 3-14c*) which were small and vastly scattered. However, 76% of *Δpor1* cells have more than 4 lipid droplets which were slightly larger than those displayed in the wild-type (*Figure 3-14d*). These results indicate that loss of porin may lead to a slight reduction in lipid droplet number after 48 hours of growth.

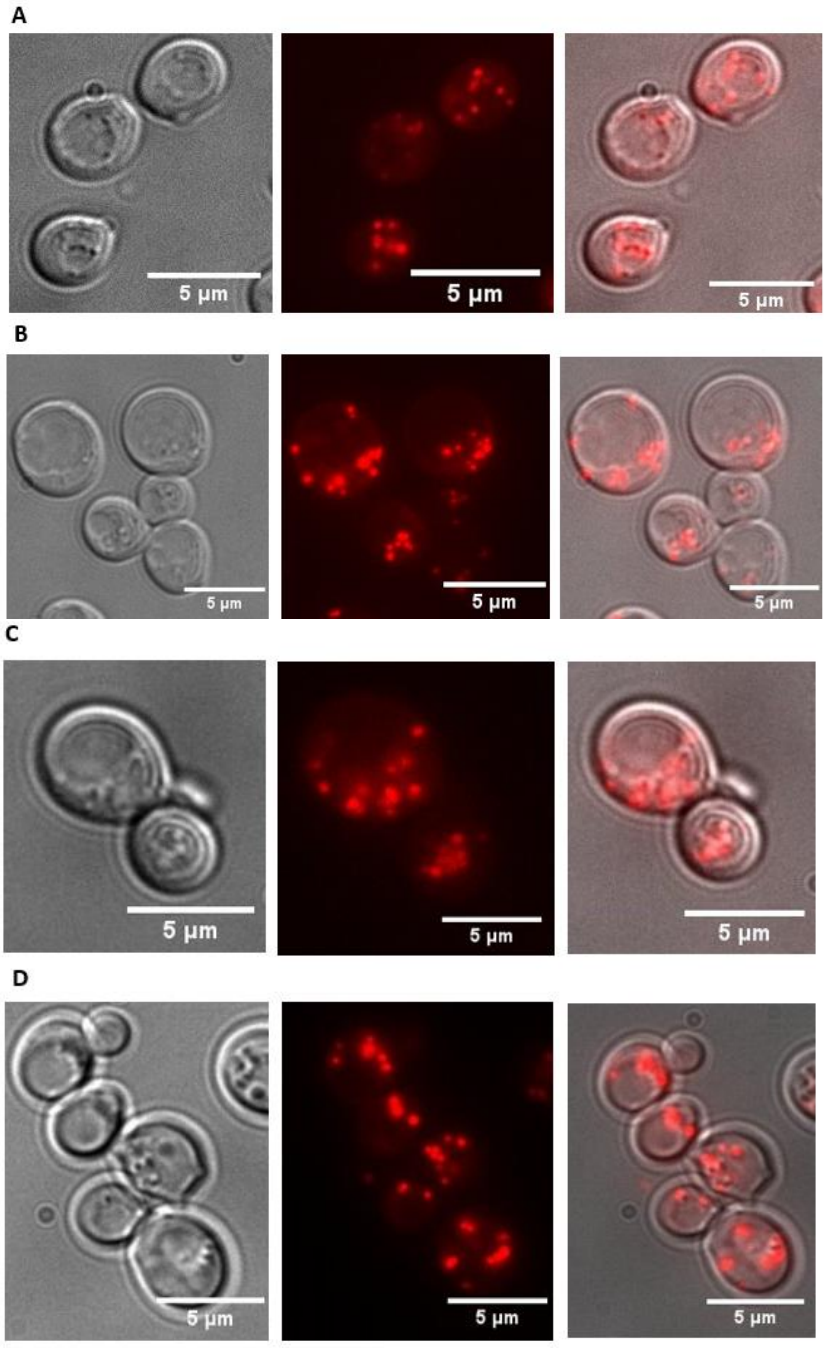


Figure 3-14: Observation of lipid droplets in wild-type and Δpor1 cells.
Wild-type and *Δpor1* cells were stained with LD450 dye and observed through fluorescence microscopy. *Δpor1* cells retained higher levels of lipid droplets at 24 hours (**B**) in comparison to wild-type cells (**A**) but displayed lower levels than the wild-type (**C**) after 48 hours (**D**). All images in grey (left) are bright field (BF), all images in the middle are RFP (fluorescence) images and all images on the right are composite.

The lipid droplet number in both wild-type and Δ*por1* cells can be seen in *Figure 3-15*. After 24 hours, wild-type and Δ*por1* cells have an average of 3.7 and 3.8 lipid doplets, respectively. After 48 hours, wild-type cells have an average of 4.6 droplets, while Δ*por1* cells have an average of 4.2.

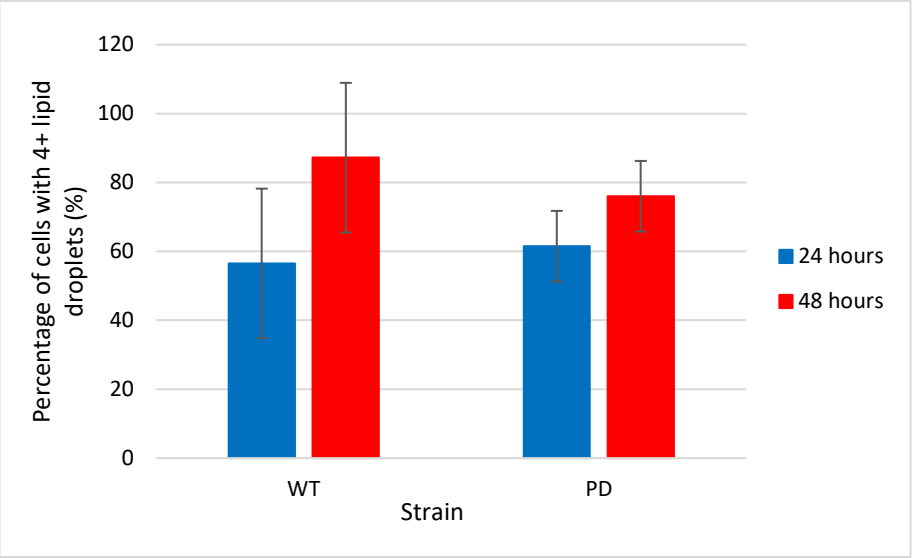


Figure 3-15: Lipid droplet number of wild-type and Δpor1 cells. Measurements of both wild-type (WT) and *Δpor1* cells (PD). This data shows that more wild-type cells have more than 4 lipid droplets in comparison to *Δpor1* cells. Error bars based on standard deviation where (n=4).

3.5.2. Loss of POR1 leads to an increase in peroxisome number

Loss of respiratory function has been linked to metabolic reprogramming via retrograde signalling[112] that is accompanied by an increase in fatty acid β-oxidation, which occurs solely within the peroxisomal compartment in *S. cerevisiae*. The peroxisome number in wild-type and porin null cells was calculated using a PTS1 (peroxisomal-targeting) SKL-GFP plasmid. Both wild-type and *Δpor1* cells were visualised at 24 hour and 48 hour growth using fluorescence microscopy (*Figure 3-16)*. After 24 hours, 6.4% of wild-type cells and 34% of *Δpor1* cells had more than 4 peroxisomes (*Figure 3-16a* and *3-16b*, respectively). After 48 hours, only 15.8% of wild-type cells had 4 or more peroxisomes per cell (*Figure 3-16c*). However, 45.1% of *Δpor1* cells had more than 4 peroxisomes per cell, a vast increase in comparison to the wild type (*Figure 3-16d*) which is also visulised in *Figure 3-17*. This data indicates an increase in peroxisome biogenesis that may support the metabolic requirements of non-respiring *Δpor1* cells.

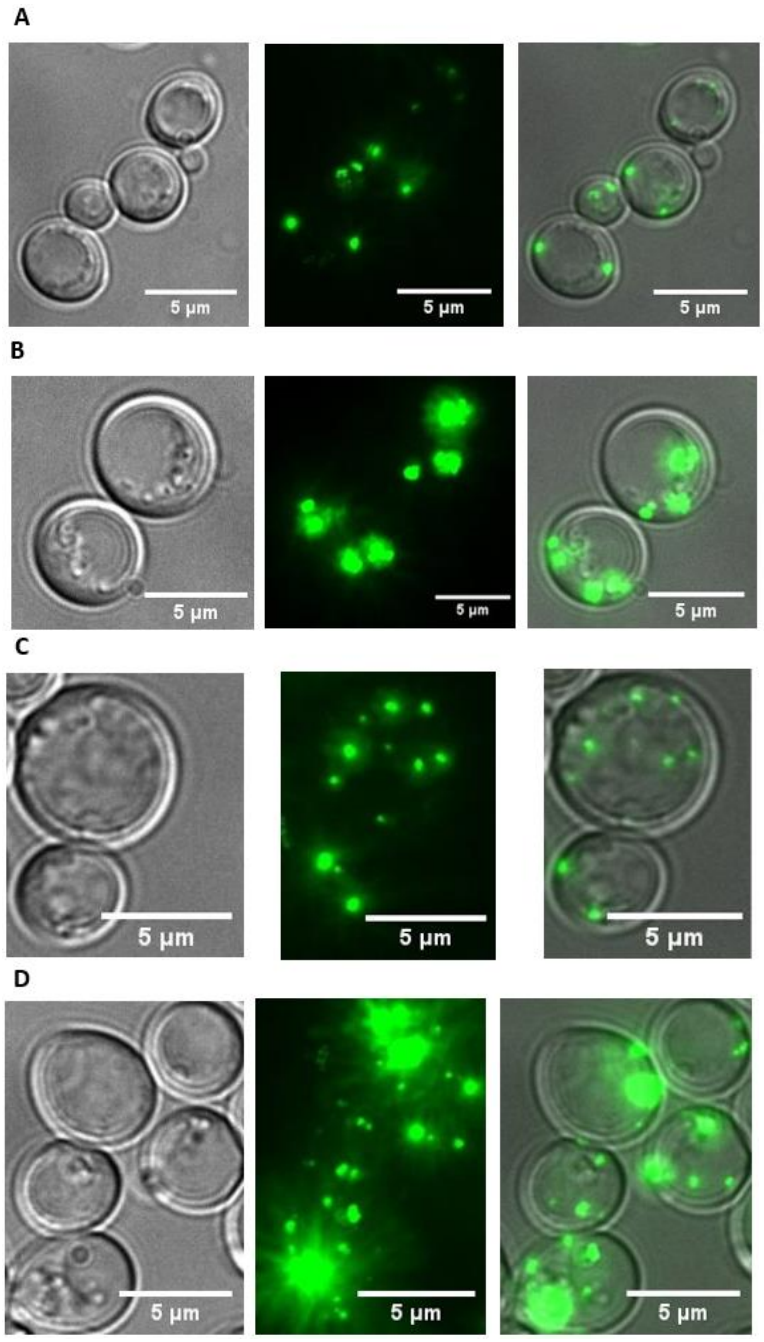


Figure 3-16: Visualisation of peroxisomes in wild-type and Δpor1 cells.
Stationary phase wild-type (**A, C**) and *Δpor1* cells (**B, D**) containing a peroxisomal-targeting SKL-GFP plasmid were visualised at 24 hours (**A, B**) and 48 hours (**C, D**) using fluorescence microscopy. Cells lacking porin have more peroxisomes per cell at both time points. All images in grey (left) are bright field (BF), all images in the middle are GFP (fluorescence) images and all images on the right are composite.

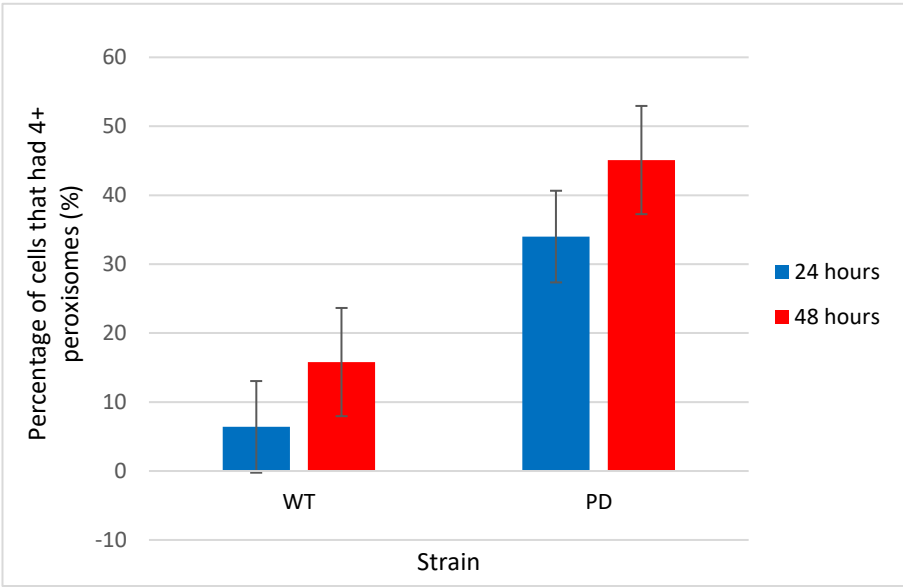


Figure 3-17: Peroxisome number of wild-type and Δpor1 cells.
Measurements of both wild-type (WT) and *Δpor1* cells (PD). This data shows that more wild-type cells have more than 4 peroxisomes in comparison to *Δpor1* cells. Error bars based on standard deviation where (n=4).

3.6 Cells lacking POR1 have a higher tendency to necrose in rich media

A loss in cell wall structure and defects in lipid homeostasis may be associated with an increase in necrotic cell death. Propidium Iodide (PI) uptake in wild-type and *Δpor1* cells was measured using flow cytometry to determine the levels of necrosis in stationary phase cells. Both wild-type and *Δpor1* cells were grown over a week in rich media (YPD) and stained with PI at regular intervals (24 hours). A small but reproducible increase in necrotic cells was observed in *Δpor1* cultures after 120 hours of growth (*Figure 3-18*). This suggests that cell wall and lipid homeostasis defects observed in Δ*por1* cells leads to a small increase in necrosis but that the majority of cells do not suffer a necrotic death.

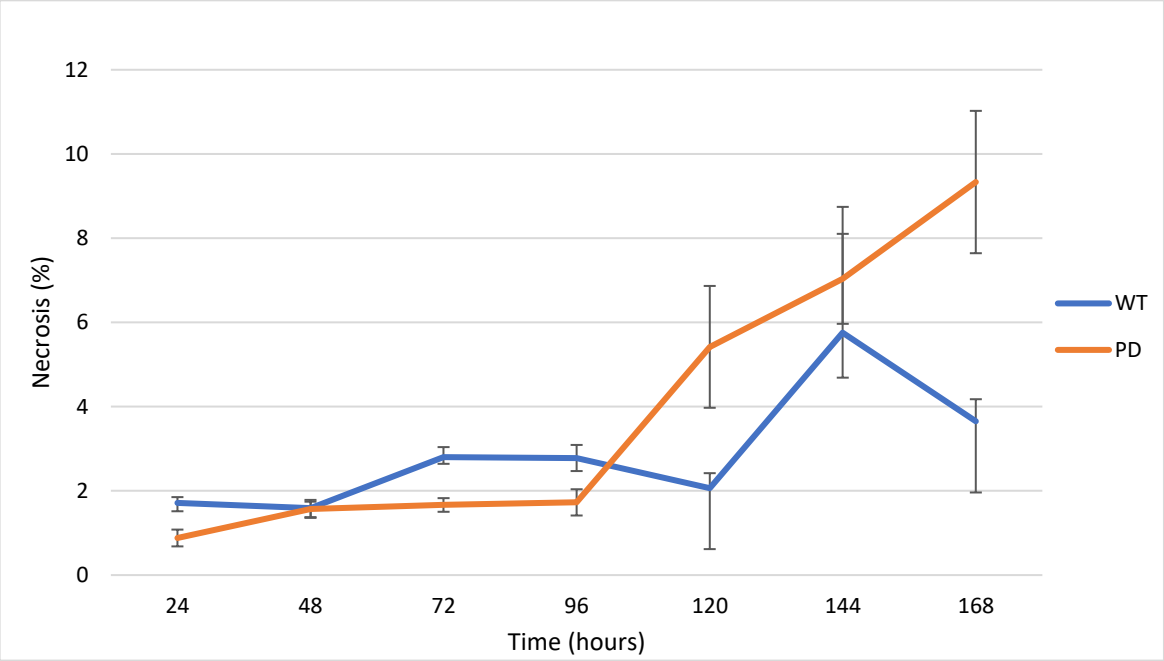


Figure 3-18: Graph displaying the necrosis levels of wild-type and Δpor1 cells in YPD media.
Values obtained through flow cytometry using PI staining as a marker for cell necrosis. Wild-type cell (WT) and *Δpor1* cell (PD) samples were analysed every 24 hours for 1 week and the resultant average values were recorded. The percentage of necrosing *Δpor1* cells is greater than that of the wildtype in YPD. Error bars based on standard deviation calculated from triplicate values (n=3).

In order to assess what effect different media has on cellular necrosis, the experiment was repeated. Firstly, both cell strains were grown over 168 hours in synthetic complete (SC) media that contained ammonium sulphate (*Section 2.1*) and readings were taken every 24 hours. In SC complete media (*Figure 3-19a*), 81.7% of wild-type cells were necrotic after 1 week, whereas only

57.5% of *Δpor1* cells were necrotic*. Figure 3-19b* shows the average necrotic values of wild-type and *Δpor1* cells grown in synthetic media over 72 hours that contains no ammonium sulphate and varying percentages of amino acid supplements (*Section 2.1* - 100%, 50%, 25%). After 72 hours, 15.7%, 10.8% and 7.85% of wild-type cells were necrotic, in 100%, 50% and 25% media, respectively. For *Δpor1* cells, 17.2%, 10.6% and 5.9% of cells were necrotic in 100%, 50% and 25% media, respectively.

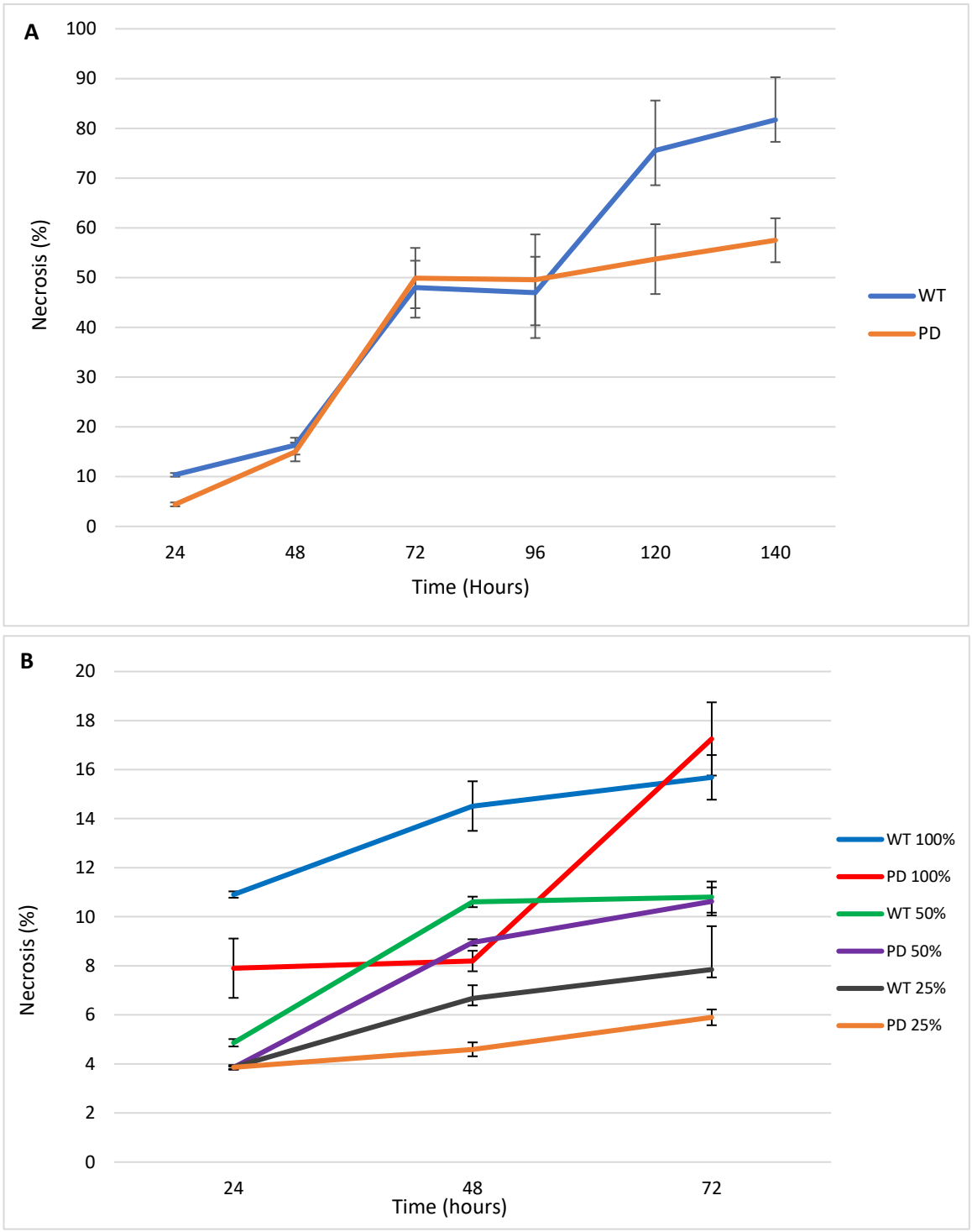


Figure 3-19: Graphs displaying the necrosis levels of wild-type and Δpor1 cells in synthetic media. Values obtained through flow cytometry using PI staining as a marker for cell necrosis. (**A**) Wild-type cell (WT) and *Δpor1* cell (PD) samples were grown in SC media and analysed over 168 hours. (**B**) Wild-type cell (WT) and *Δpor1* cell (PD) samples were grown in synthetic media (SC) without ammonium sulphate and varying nutrient levels and analysed over 72 hours. (100%) = cells grown in media with 100% of the required nutrients, (50%) = cells grown in media containing 50% of the required nutrients, (25%) = cells grown in media containing 25% of the required nutrients. Error bars based on standard deviation calculated from triplicate values (n=3). The percentage of necrosing *Δpor1* cells is generally lower than that of the wildtype in all the synthetic media trialled.

These results show that in more selective media, cells lacking porin are, on average, less necrotic than that of the wild type and the level of necrosis in Δ*por1* cells is much higher in SD-URA media

than wild type, as shown by the y-axis in these two figures. Reducing the level of amino acid supplement and ammonium sulphate greatly reduces the levels of necrosis in SD-URA media, which may be caused by slower growth.

3.7 Overexpression of POR1

Cells containing a porin overexpression plasmid (PCG633) were also investigated to see whether; a) the phenotypes of *Δpor1* cells could be reversed b) the effects of elevated levels of POR1 on cell fitness. To confirm that porin is overexpressed in cells containing the porin overexpression plasmid, a western blot was carried out to detect the levels of porin in wild-type, *Δpor1* and *Δpor1* cells containing a porin overexpression plasmid, as shown in *Figure 3-20*.

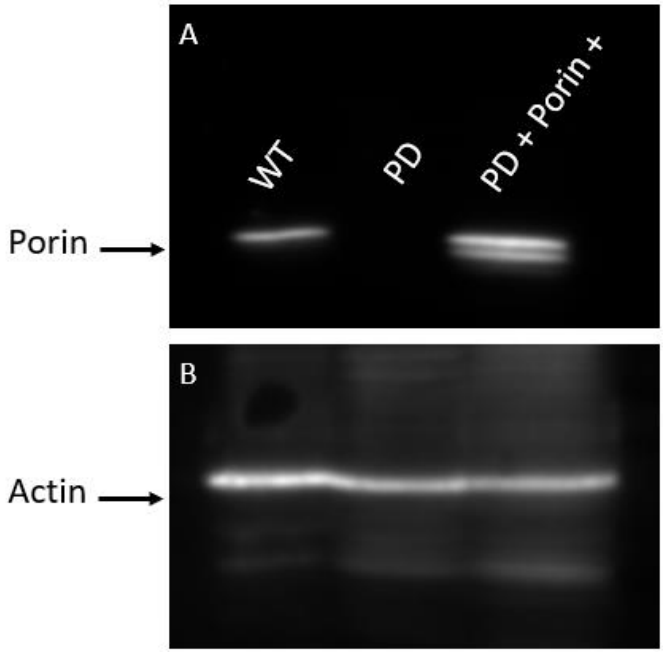


Figure 3-20: Western blot showing the levels of porin in S. cerevisiae. **A**) The levels of porin in wild-type (WT), *Δpor1 (PD*) and Δ*por1* cells containing an overexpression plasmid (PD + Porin +). Porin is abundant in cells with the overexpression plasmid. **B**) Actin loading control displaying the levels of loaded protein.

3.7.1 Porin overexpression leads to an increase in necrosis

As the loss of porin appeared to influence the level of necrosis observed in culture we investigated the effects of POR1 overexpression on PI uptake using flow cytometry (*Figure 3-21)*. Both wild-type and *Δpor1* cells that overexpress porin were grown in SD-URA and analysed at regular intervals for 72 hours. In both backgrounds the introduction of a POR1 overexpression plasmid led to a significant increase in necrosis, with 48.5% of *Δpor1* cells and 70.1% of wild-type cells that had a porin overexpression plasmid becoming necrotic after 72 hours (*Figure 3-21*). Wild-type and *Δpor1*

cells that had an empty control plasmid showed 25.6% and 28.7% necrosis at 72 hours, respectively. This data suggests that an increase in the level of porin is sufficient to drive a necrotic form of cell death.

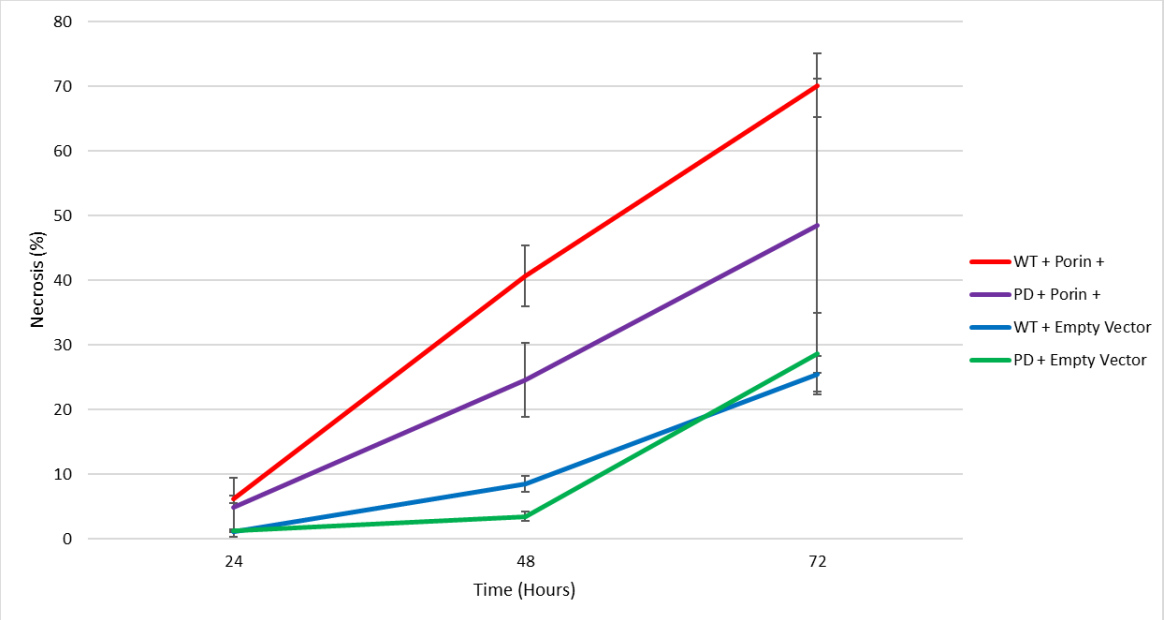


Figure 3-21: Graph displaying the necrosis levels of cells that overexpress porin in SD-URA.
Values obtained through flow cytometry using PI staining as a marker for cell necrosis. Wild-type cell (WT) and *Δpor1* cell (PD) samples were analysed at regular intervals for 72 hours and the resultant average values were recorded. (Porin +) = cells contain a plasmid that overexpresses porin. Wild-type and Δpor1 cells transformed with an empty vector were used as a control (Empty Vector). Error bars based on standard deviation calculated from triplicate values (n=3).

3.7.2 Flocculation and Cell Wall Integrity pathway activation occurs when porin is overexpressed

We observed that overexpression of POR1 led to the aggregation of cells, or flocculation, in overnight cultures (*Figure 3-22)*. Overnight cultures of both wild-type and Δ*por1* cells containing an empty vector plasmid (*Figure 3-22c, d*) were compared to cells containing a porin overexpression plasmid (*Figure 3-22e, f*). Rho zero (Rho°) cells and Δ*cox4* strains transformed with a porin overexpression plasmid (*Figure 3-22g, h*) were included to confirm that any flocculation seen was based on porin expression, as both Rho° and Δ*cox4* cells are also respiratory deficient. Rho° cells do not contain any mitochondrial DNA (mtDNA), and Δ*cox4* cells lack the cytochrome *c* oxidase subunit IV. Flocculation can occur as a result of activation of the MAPK CWI. If porin is involved in this pathway it may also help to explain the reduced cell wall thickness observed in *Figure 3-13*. Activation of the CWI pathway can be assessed by measuring the phosphorylation status of the terminal MAPK, Stl2.

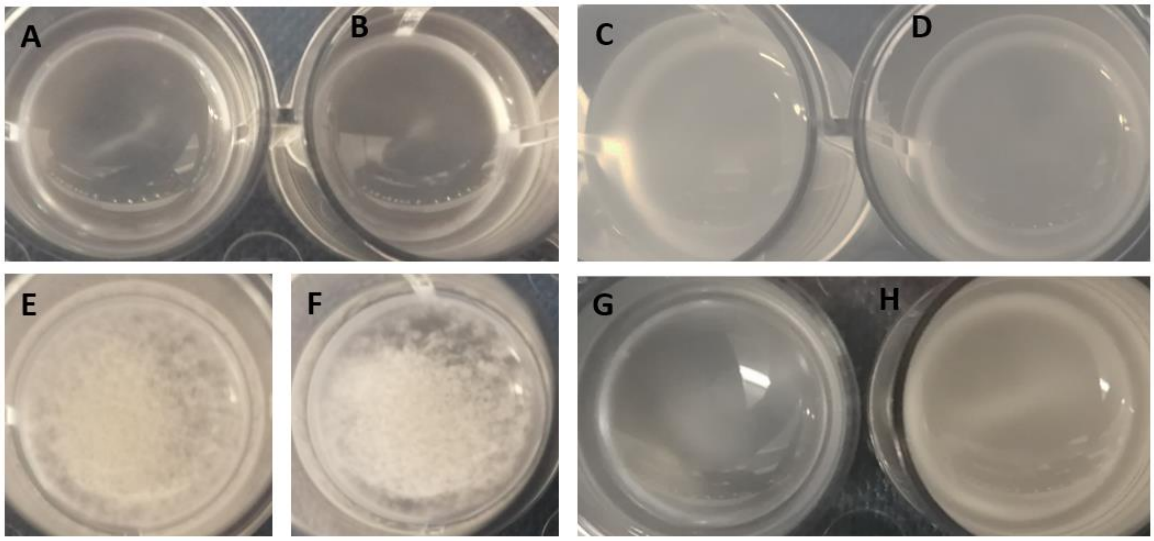


Figure 3-22: Overnight cultures of cells that overexpress porin show flocculation.
Overnight cultures of (**A**) wild-type (**B**) Δ*por1* cells were compared to wild-type and Δ*por1* cells transformed with an empty vector plasmid (**C** and **D**, respectively) and wild-type (**E**) and Δ*por1* cells (**F**) containing a porin overexpression plasmid. Cells that overexpress porin flocculate. Overnight cultures of Rho° cells (**G**) and Δ*cox4* cells (**H**) containing a porin overexpression plasmid were grown as a plasmid control.

To confirm whether the CWI pathway is being activated upon POR1 overexpression, a western blot probing for phosphorylated Slt2 was carried out. Cell lysate from wild-type, Δ*por1* cells, and cells that have an overexpression plasmid can be seen in *Figure 3-23*. Calcofluor White stress (CFW) was used as a positive control to activate the CWI pathway. The blot confirms that cells that overexpress porin have higher levels of phosphorylated Slt2 as there is a thicker, brighter band present which mirrors the positive control.

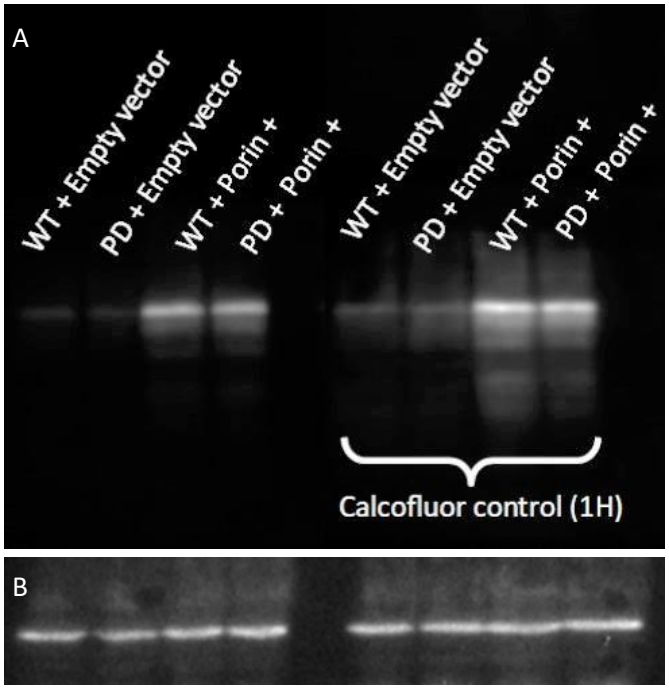


Figure 3-23: Western blot showing the levels of phosphorylated Slt2 in cells that overexpress porin.
A) Samples of wild-type (WT) and *Δpor1* (PD) cells containing a porin overexpression plasmid (Porin +) and an empty vector plasmid (Empty Vector) were analysed to confirm whether porin overexpression leads to Slt2 activation. A calcofluor stress was added to samples for one hour as a positive control. **B**) Actin loading control displaying the levels of loaded protein.

3.7.3 Cells that overexpress porin lack vacuolar integrity and may have an endocytosis defect

Slt2 activity is known to affect vacuole function and morphology[113]. Considering that cells that overexpress porin show an increase in phosphorylated Slt2, FM4-64 staining of cells that overexpress porin was carried out in order to examine the effects of overexpression on vacuolar morphology. *Δpor1* cells containing a porin overexpression plasmid were stained during stationary phase and observed using fluorescence microscopy, as seen in *Figure 3-24.* The results of the vacuolar staining showed that 35% of cells displayed fragmented vacuoles (seen in *Figure 3-24a*) and 65% displayed the dye on the outer wall of the cell rather than the vacuole, indicating an endocytosis defect (*Figure 3-24b*).

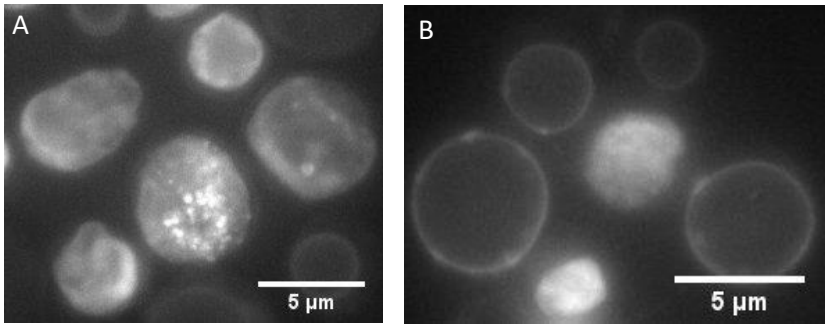


Figure 3-24: Vacuolar structure of cells containing a porin overexpression plasmid.
Vacuolar staining (using FM4-64) of porin overexpression cells in stationary phase showed either vacuolar fragmentation (**A**) or an endocytosis defect in which only the plasma membrane was stained (**B**). This indicates that overexpression of porin may regulate components that affect cell wall integrity.

These data confirmed that porin overexpression affects vacuolar integrity and leads to a strong defect in membrane internalisation.

4. Discussion

4.1 Loss of porin leads to a change in mitochondrial morphology and loss of respiration

Here, we show that cells lacking porin develop aggregated mitochondria with a respiratory defect. This data indicates that porin is crucial for mitochondrial structure and function. One possibility is that a loss of porin reduces the influx of compounds that may be used to support respiration, such as glucose. Another possibility is that porin is associated with the ERMES complex; this is supported by the fact that loss of ERMES components gives rise to the same aggregation phenotype[114-116]. One possibility is that porin interacts with Mdm34. This is because the mechanism through which Mdm34 interacts with the outer mitochondrial membrane is still unknown. As porin is abundant, it represents a putative binding target of Mdm34. A severance in this bond through a loss of porin could therefore lead to a collapse of the mitochondrial outer membrane, developing an aggregated phenotype displayed in *Section 3.1*. To test this, co-immunoprecipitation experiments could be carried out to assess whether porin1 and Mdm34 are associated.

4.2 Both loss and overexpression of POR1 results in growth defects and necrosis

After assessing that *Δpor1* cells had a respiratory defect, an investigation into their growth patterns was carried out. The results showed that porin null cells grown in glucose reached a lower OD than the wild type which plateaued in stationary phase, whereby a loss of respiration caps cellular growth. In media containing glycerol, however, *Δpor1* cells did not reach exponential growth. This is because glycerol is a non-fermentable carbon source and dehydrogenation through glycerol-3-phosphate dehydrogenase (GlpD) is required to shuttle electrons into the respiratory transport chain[117]. This means that *Δpor1* cells cannot utilise glycerol which indicates that porin1 is essential for mitochondrial glycerol uptake. Cells that re-express porin, however, show stronger growth with less of a plateau in stationary phase in glucose and can also grow better in the presence of glycerol than *Δpor1* cells. Cells that contained an empty vector plasmid in glycerol displayed a long lag phase and a higher exponential growth than cells containing a porin overexpression plasmid, which indicated that these cells may have been undergoing a diauxic shift and transcriptional

reprogramming to upregulate the genes required to utilise non fermentable carbon sources[118]. However, while porin re-expression increases cellular growth, neither the re-expression nor the *Δpor1* cells grow to the same OD as the wild type. This confirms that while porin is essential for respiration which produces healthy cellular growth, both loss and overexpression of porin leads to growth defects.

In order to establish the effects of porin loss and overexpression on cell death, PI was used as a marker for cellular necrosis. Interestingly, around 10% of Δ*por1* cells were necrotic in rich media, whereby most cells did not take up the PI. In SD-URA, however, the level of necrosis increased significantly, although a reduction in amino acid levels in the media reduced the number of necrotic cells present. The necrotic phenotype displayed by Δ*por1* cells may be in part due to the alterations of lipid compositions seen in the cell walls. Because we have seen that cells lacking porin have thinner cell walls than wild type, it is tempting to speculate that the change in lipid composition presents a weakness in the cell wall, which would lead to necrosis. However, because PI is only a marker of necrosis, and not other types of cell death such as autophagy, it may be that a loss of porin leads to a loss of viability by other means. To test this, experiments such as Colony Forming Unit assays (CFU) could be carried out to assess cell viability over time. Cells that overexpressed porin, however, were also necrotic, which may be linked to the cell wall changes that underlie flocculation seen in overnight cultures. To test this, we could expose cells to cell wall stresses, such as CFW and determine the effect this has on necrosis levels of cells that overexpress porin.

4.3 Cells lacking porin exhibit lower autophagy levels and altered lipidomics

A reduction in ATG8-GFP levels displayed in *Δpor1* cells in *Section 3.4.1* indicates that cells lacking porin may have a defect in autophagy and a reduction in autophagosome formation. This is because the levels of free GFP in the vacuoles of *Δpor1* cells indicated that there was a disruption either in the signal to activate autophagy or in processing of autophagosomes at the vacuole as part of the autophagy process. As we have seen in *Section 3.4.2*, the lack of autophagic activity in *Δpor1* cells was not attributable to vacuolar integrity; which confirms that the lack of observable ATG8-GFP could have been attributed to a change in the autophagy pathway itself.

While we have seen that autophagy proteins such as Atg1, Atg13, Atg17, Atg29 and Atg31 are key for autophagosome formation, Atg8 is a crucial component of this process through covalent bondage to PE on autophagosomal membranes, which indirectly tethers Atg1 to the autophagosomal membrane via an AIM[82]. Investigations into the lipid composition of the inner and outer membranes of *Δpor1* cells with Dr Patrick Rockenfeller (University of Graz) and Dr. Oskar Knittelfelder (Max Planck Institute of Molecular Cell Biology and Genetics (MPI-CBG) Dresden, Germany showed that fatty acid levels were altered in porin mutant cells (*Section 3.5*). A particularly striking example was PS, PE and PC, as these lipids are modified through the ER-mitochondrial connection and are reliant on membrane associated enzymes in both organelles. An observable increase in levels of PS and PC but a reduction in PE supports the idea that porin is associated with ERMES and that a loss of porin severs the ER-mitochondrial connection. This is because the primary source of PS is localised in the ER, and a loss of ERMES connection would result in a loss of transfer of PS to the OMM for decarboxylation by Psd1, to form PE. The increase in PC, however, may be due to an accumulation of cellular substrates as there are multiple PC biogenesis pathways, such as condensation of diacylglycerols with cytidine 5'-diphosphocholine (CDP choline)[119]**.**

The lack of PE observed in *Δpor1* cells may in part explain the autophagic phenotype displayed in *Section 3.4*. This is because a reduction in PE through the severance of ERMES would then cause a reduction in the lipid for autophagosomal membrane use. It would be reasonable to suggest, therefore, that removal of porin breaks the ERMES connection, resulting in lowered PE levels and reduction of autophagosome formation due to the inability of Atg8 to bond with the autophagosomal membrane. In order to test this, double immunofluorescence or co-immunoprecipitation experiments could be used to examine a co-distribution of Atg8 with PE in Δ*por1* cells.

4.4 Loss of POR1 leads to increased lipid storage and peroxisome number

While the reduction in PE specifically can be linked to Atg8 connection to autophagosomes, the levels of lipid droplets and peroxisomes were investigated. This is because a change in lipid

homeostasis and composition of the cell membranes indicated that the autophagy defect observed by *Δpor1* cells could also be based on redirection of lipids as a result of ERMES disconnection. As observed in *Section 3.5*, *Δpor1* cells had an initial increase of lipid droplets, which reduced over 48 hours in comparison to the wild type. The peroxisome number of *Δpor1* cells, however, was a lot higher than the wild type over 48 hours. These results indicate that an alteration in lipid biosynthesis, such as PS and PC, may increase lipid storage initially, but these fatty acids may be shuttled through retrograde signalling to peroxisomes for β-oxidation. This peroxisome specific oxidation is used to generate components such as Acetyl-CoA to aleviate the mitochondrial respitory deficiency characteristic of porin null mutants. A similar shift in metabolism is also seen in Rho zero cells and is regulated by retrograde signalling[120].

4.5 Overexpression of porin leads to increased components of the cell wall integrity pathway

Observation of overnight cultures of cells that overexpress POR1 resulted in flocculation. This indicated that porin may be involved in the CWI and to investigate this an assessment of the vacuolar integrity of these cells was carried out. Upon staining with FM4-64, the two phenotypes that were presented were fragmented vacuoles and observation of the dye on the plasma membrane. The result shown in *Figure 3-20* indicated that cells that overexpressed porin had an endocytosis defect to some degree; that is, the dye could not be endocytosed properly and sat on the outer membrane instead. This may be because while a loss of porin leads to a thinner plasma membrane with altered lipid composition, one could speculate that an overexpression of porin would also lead to altered cell membranes which may not be able to form endocytotic vesicles. The vacuole fragmentation, however, confirmed that porin overexpression may signal to CWI components as Slt2, the yeast MAP kinase, which is known to play a role in actin remodelling and vacuolar morphology[113]. This theory was confirmed through the observation of increased phosphorylated (active) Slt2 in porin overexpression strains on a western blot. One could conclude, therefore, that porin is involved in the CWI pathway, by perhaps acting as a scaffold for Slt2 phosphorylation. Overexpression in this case would have therefore increased the levels of active

Slt2, leading to vacuole fragmentation, increased cell wall repair and flocculation (*Figure 4-1*). It should also be noted that loss of porin could lead to reduced Slt2 activation of autophagy, which may contribute to the autophagy defect seen in Δ*por1* cells.

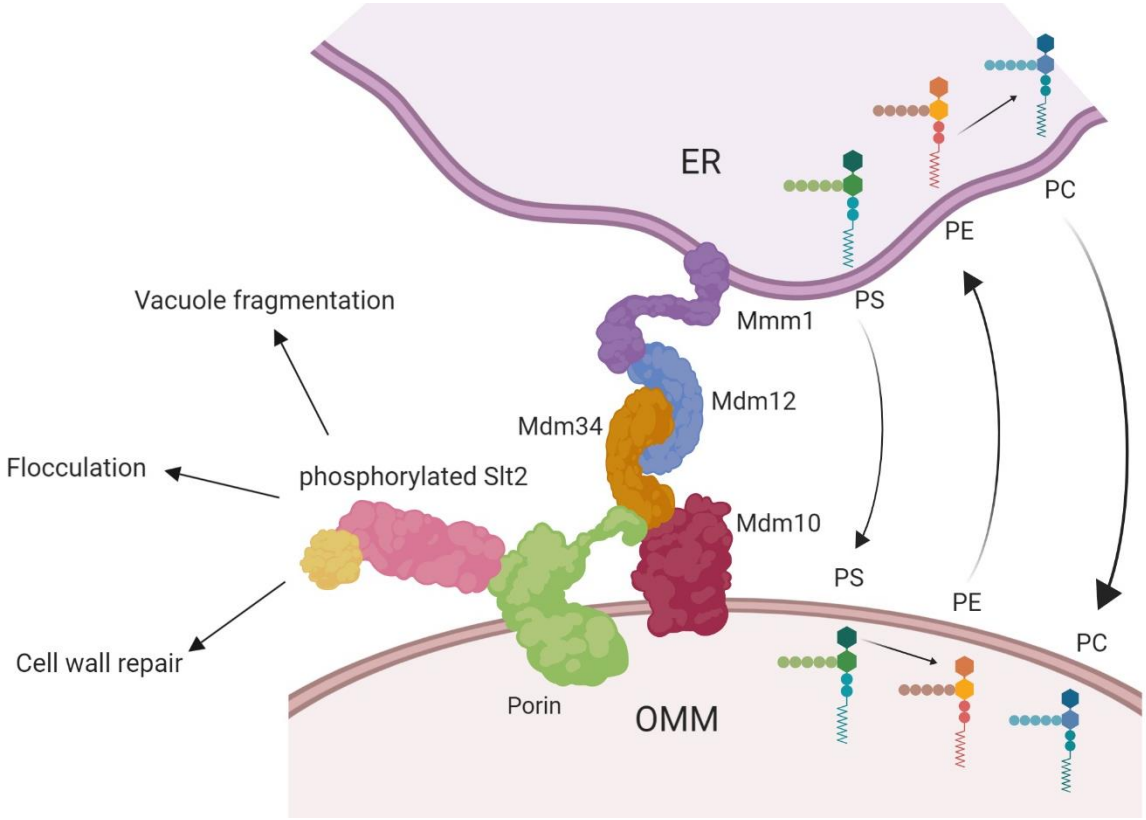


Figure 4-1: Schematic illustrating the potential roles of porin.
Porin1 may be associated with the ERMES complex through binding to Mdm34, which maintains respiration and a healthy mitochondrial morphology. The lipid maturation pathway between the ER and the mitochondria will remain intact through the porin-ERMES connection. Porin may also serve as a scaffold for Slt2 activation which in turn promotes flocculation, cell wall repair, and vacuole fragmentation. PS = Phosphatidylserine, PE = Phosphatidylethanolamine, PC = Phosphatidylcholine. Adapted from Osman et.al[121] and made with BioRender.com.

4.6 Final remarks and future directions

In conclusion, we hypothesise that porin1 is associated with the ERMES complex, potentially through interaction with Mdm34, and that this association is required to maintain mitochondrial morphology and respiratory function. One can also speculate that this porin-ERMES linkage facilitates the movement of lipids between the two organelles for efficient lipid homeostasis and healthy cell membrane lipid composition. Furthermore, our studies show that porin may be a scaffold for Slt2 activation which in turn activates the cell wall integrity pathway and leads to cell wall repair, flocculation and vacuole fragmentation. This evidence highlights porin to be a viable

drug target for fungal infections as a loss of this channel leads to unfit growth patterns and a loss of cell wall integrity. Drugs that could target porin in combination with other antifungal therapies may present an alternative solution to antifungal resistance.

5. References

1. Tsujimoto Y, Shimizu S. (2007) Role of the mitochondrial membrane permeability transition in cell death. *Apoptosis*. 12(5):835-840. https://doi.org/10.1007/s10495-006-0525-7. doi: 10.1007/s10495-006-0525-7.

2. Bayrhuber M, Meins T, Habeck M, et al. (2008) Structure of the human voltage-dependent anion channel. *Proc Natl Acad Sci U S A*. 105(40):15370-15375. doi: 10.1073/pnas.0808115105 [doi].

3. Mannella CA, Bonner WD,Jr. (1975) Biochemical characteristics of the outer membranes of plant mitochondria. *Biochim Biophys Acta*. 413(2):213-225. doi: 0005-2736(75)90105-4 [pii].

4. Schein SJ, Colombini M, Finkelstein A. (1976) Reconstitution in planar lipid bilayers of a voltage-dependent anion-selective channel obtained from paramecium mitochondria. *J Membr Biol*. 30:99-120.

5. Reina S, Palermo V, Guarnera A, et al. (2010) Swapping of the N-terminus of VDAC1 with VDAC3 restores full activity of the channel and confers anti-aging features to the cell. *FEBS Lett*. 584(13):2837-2844. doi: 10.1016/j.febslet.2010.04.066 [doi].

6. Catia Sorgato M, Moran O, Pedersen PL. (1993) Channels in mitochondrial membranes: Knowns, unknowns, and prospects for the future. *Crit Rev Biochem Mol Biol*. 28(2):127-171. https://doi.org/10.3109/10409239309086793. doi: 10.3109/10409239309086793.

7. Young MJ, Bay DC, Hausner G, Court DA. (2007) The evolutionary history of mitochondrial porins. *BMC Evol Biol*. 7:31-2148-7-31. doi: 1471-2148-7-31 [pii].

8. Ujwal R, Cascio D, Colletier JP, et al. (2008) The crystal structure of mouse VDAC1 at 2.3 A resolution reveals mechanistic insights into metabolite gating. *Proc Natl Acad Sci U S A*. 105(46):17742-17747. doi: 10.1073/pnas.0809634105 [doi].

9. Hiller S, Garces RG, Malia TJ, Orekhov VY, Colombini M, Wagner G. (2008) Solution structure of the integral human membrane protein VDAC-1 in detergent micelles. *Science*. 321(5893):1206-1210. doi: 10.1126/science.1161302 [doi].

10. Triphan X, Menzel VA, Petrunkina AM, et al. (2008) Localisation and function of voltage-dependent anion channels (VDAC) in bovine spermatozoa. *Pflugers Arch*. 455(4):677-686. doi: 10.1007/s00424-007-0316-1 [doi].

11. Xu X, Decker W, Sampson MJ, Craigen WJ, Colombini M. (1999)Mouse VDAC isoforms expressed in yeast: Channel properties and their roles in mitochondrial outer membrane permeability. *J Membr Biol*. 170(2):89-102. doi: JMEMB065 [pii].

12. Colombini M. (2004) VDAC: The channel at the interface between mitochondria and the cytosol. *Mol Cell Biochem*. 256-257(1-2):107-115.

13. Blachly-Dyson E, Forte M. (2001) VDAC channels. *IUBMB Life*. 52(3-5):113-118. doi: 10.1080/15216540152845902 [doi].

14. De Pinto V, Messina A, Accardi R, et al. (2003) New functions of an old protein: The eukaryotic porin or voltage dependent anion selective channel (VDAC). *Ital J Biochem*. 52(1):17-24.

15. Rostovtseva TK, Tan W, Colombini M. (2005) On the role of VDAC in apoptosis: Fact and fiction. *J Bioenerg Biomembr*. 37(3):129-142. doi: 10.1007/s10863-005-6566-8 [doi].

16. Keinan N, Tyomkin D, Shoshan-Barmatz V. (2010) Oligomerization of the mitochondrial protein voltage-dependent anion channel is coupled to the induction of apoptosis. *Mol Cell Biol*. 30(24):5698-5709. doi: 10.1128/MCB.00165-10 [doi].

17. Rostovtseva T, Colombini M. (1996) ATP flux is controlled by a voltage-gated channel from the mitochondrial outer membrane. *J Biol Chem*. 271(45):28006-28008.

18. Karachitos A, Galganska H, Wojtkowska M, et al. (2009) Cu,zn-superoxide dismutase is necessary for proper function of VDAC in saccharomyces cerevisiae cells. *FEBS Lett*. 583(2):449-455. doi: 10.1016/j.febslet.2008.12.045 [doi].

19. Bathori G, Csordas G, Garcia-Perez C, Davies E, Hajnoczky G. (2006) Ca2+-dependent control of the permeability properties of the mitochondrial outer membrane and voltage-dependent anion-selective channel (VDAC). *J Biol Chem*. 281(25):17347-17358. doi: M600906200 [pii].

20. Bera AK, Ghosh S. (2001) Dual mode of gating of voltage-dependent anion channel as revealed by phosphorylation. *J Struct Biol*. 135(1):67-72. doi: 10.1006/jsbi.2001.4399 [doi].

21. Gurnev PA, Queralt-Martin M, Aguilella VM, Rostovtseva TK, Bezrukov SM. (2012) Probing tubulin-blocked state of VDAC by varying membrane surface charge. *Biophys J*. 102(9):2070-2076. doi: 10.1016/j.bpj.2012.03.058 [doi].

22. Krimmer T, Rapaport D, Ryan MT, et al. (2001) Biogenesis of porin of the outer mitochondrial membrane involves an import pathway via receptors and the general import pore of the TOM complex. *J Cell Biol*. 152(2):289-300.

23. Kozjak-Pavlovic V, Ross K, Benlasfer N, Kimmig S, Karlas A, Rudel T. (2007) Conserved roles of Sam50 and metaxins in VDAC biogenesis. *EMBO Rep*. 8(6):576-582. doi: 7400982 [pii].

24. Crompton M. (1999) The mitochondrial permeability transition pore and its role in cell death. *Biochem J*. 341 (Pt 2)(Pt 2):233-249.

25. Marzo I, Brenner C, Zamzami N, et al. (1998) Bax and adenine nucleotide translocator cooperate in the mitochondrial control of apoptosis. *Science*. 281(5385):2027-2031.

26. Zoratti M, Szabo I. (1995) The mitochondrial permeability transition. *Biochim Biophys Acta*. 1241(2):139-176. doi: 0304-4157(95)00003-A [pii].

27. Veenman L, Shandalov Y, Gavish M. (2008) VDAC activation by the 18 kDa translocator protein (TSPO), implications for apoptosis. *J Bioenerg Biomembr*. 40(3):199-205. doi: 10.1007/s10863-008-9142-1 [doi].

28. Schlattner U, Dolder M, Wallimann T, Tokarska-Schlattner M. (2001) Mitochondrial creatine kinase and mitochondrial outer membrane porin show a direct interaction that is modulated by calcium. *J Biol Chem*. 276(51):48027-48030. doi: 10.1074/jbc.M106524200 [doi].

29. Baines CP, Kaiser RA, Sheiko T, Craigen WJ, Molkentin JD. (2007) Voltage-dependent anion channels are dispensable for mitochondrial-dependent cell death. *Nat Cell Biol*. 9(5):550-555. doi: ncb1575 [pii].

30. Baines CP, Kaiser RA, Purcell NH, et al. (2005) Loss of cyclophilin D reveals a critical role for mitochondrial permeability transition in cell death. *Nature*. 434(7033):658-662. doi: nature03434 [pii].

31. Kokoszka JE, Waymire KG, Levy SE, et al. (2004) The ADP/ATP translocator is not essential for the mitochondrial permeability transition pore. *Nature*. 427(6973):461-465. doi: 10.1038/nature02229 [doi].

32. Schinzel AC, Takeuchi O, Huang Z, et al. (2005) Cyclophilin D is a component of mitochondrial permeability transition and mediates neuronal cell death after focal cerebral ischemia. *Proc Natl Acad Sci U S A*. 102(34):12005-12010. doi: 0505294102 [pii].

33. Nakagawa T, Shimizu S, Watanabe T, et al. (2005) Cyclophilin D-dependent mitochondrial permeability transition regulates some necrotic but not apoptotic cell death. *Nature*. 434(7033):652-658. doi: nature03317 [pii].

34. Nesci S, Trombetti F, Ventrella V, Pagliarani A. (2018) From the Ca2+-activated F1FO-ATPase to the mitochondrial permeability transition pore: An overview. *Biochimie*. 152:85-93. doi: https://doi.org/10.1016/j.biochi.2018.06.022.

35. Marin R, Ramirez CM, Gonzalez M, et al. (2007) Voltage-dependent anion channel (VDAC) participates in amyloid beta-induced toxicity and interacts with plasma membrane estrogen receptor alpha in septal and hippocampal neurons. *Mol Membr Biol*. 24(2):148-160. doi: 777457410 [pii].

36. Ramirez CM, Gonzalez M, Diaz M, et al. (2009) VDAC and ERalpha interaction in caveolae from human cortex is altered in alzheimer's disease. *Mol Cell Neurosci*. 42(3):172-183. doi: 10.1016/j.mcn.2009.07.001 [doi].

37. Mello CF, Sultana R, Piroddi M, et al. (2007) Acrolein induces selective protein carbonylation in synaptosomes. *Neuroscience*. 147(3):674-679. doi: S0306-4522(07)00461-7 [pii].

38. Cuadrado-Tejedor M, Vilarino M, Cabodevilla F, Del Rio J, Frechilla D, Perez-Mediavilla A. (2011) Enhanced expression of the voltage-dependent anion channel 1 (VDAC1) in alzheimer's disease transgenic mice: An insight into the pathogenic effects of amyloid-beta. *J Alzheimers Dis*. 23(2):195-206. doi: 10.3233/JAD-2010-100966 [doi].

39. Sun Y, Vashisht AA, Tchieu J, Wohlschlegel JA, Dreier L. (2012) Voltage-dependent anion channels (VDACs) recruit parkin to defective mitochondria to promote mitochondrial autophagy. *J Biol Chem*. 287(48):40652-40660. doi: 10.1074/jbc.M112.419721 [doi].

40. Shimizu S, Matsuoka Y, Shinohara Y, Yoneda Y, Tsujimoto Y. (2001) Essential role of voltage-dependent anion channel in various forms of apoptosis in mammalian cells. *J Cell Biol*. 152(2):237-250.

41. Sugiyama T, Shimizu S, Matsuoka Y, Yoneda Y, Tsujimoto Y. (2002) Activation of mitochondrial voltage-dependent anion channel by apro-apoptotic BH3-only protein bim. *Oncogene*. 21(32):4944-4956. doi: 10.1038/sj.onc.1205621 [doi].

42. Yuan S, Fu Y, Wang X, et al. (2008) Voltage-dependent anion channel 1 is involved in endostatin-induced endothelial cell apoptosis. *FASEB J*. 22(8):2809-2820. doi: 10.1096/fj.08-107417 [doi].

43. Chen Y, Craigen WJ, Riley DJ. (2009) Nek1 regulates cell death and mitochondrial membrane permeability through phosphorylation of VDAC1. *Cell Cycle*. 8(2):257-267. doi: 7551 [pii].

44. Abu-Hamad S, Zaid H, Israelson A, Nahon E, Shoshan-Barmatz V. (2008) Hexokinase-I protection against apoptotic cell death is mediated via interaction with the voltage-dependent anion channel-1: Mapping the site of binding. *J Biol Chem*. 283(19):13482-13490. doi: 10.1074/jbc.M708216200 [doi].

45. Thomas L, Blachly-Dyson E, Colombini M, Forte M. (1993) Mapping of residues forming the voltage sensor of the voltage-dependent anion-selective channel. *Proc Natl Acad Sci U S A*. 90(12):5446-5449.

46. Song J, Midson C, Blachly-Dyson E, Forte M, Colombini M. (1998)The sensor regions of VDAC are translocated from within the membrane to the surface during the gating processes. *Biophys J*. 74(6):2926-2944. doi: S0006-3495(98)78000-2 [pii].

47. Ujwal R, Cascio D, Chaptal V, Ping P, Abramson J. (2009) Crystal packing analysis of murine VDAC1 crystals in a lipidic environment reveals novel insights on oligomerization and orientation. *Channels (Austin)*. 3(3):167-170. doi: 9196 [pii].

48. Zalk R, Israelson A, Garty ES, Azoulay-Zohar H, Shoshan-Barmatz V. (2005) Oligomeric states of the voltage-dependent anion channel and cytochrome c release from mitochondria. *Biochem J*. 386(Pt 1):73-83. doi: 10.1042/BJ20041356 [doi].

49. Lang A, John Peter AT, Kornmann B. (2015) ER-mitochondria contact sites in yeast: Beyond the myths of ERMES. *Curr Opin Cell Biol*. 35:7-12. doi: 10.1016/j.ceb.2015.03.002 [doi].

50. Smethurst DGJ, Cooper KF. (2017) ER fatalities-the role of ER-mitochondrial contact sites in yeast life and death decisions. *Mech Ageing Dev*. 161(Pt B):225-233. doi: S0047-6374(16)30113-0 [pii].

51. Michel AH, Kornmann B. (2012) The ERMES complex and ER-mitochondria connections. *Biochem Soc Trans*. 40(2):445-450. doi: 10.1042/BST20110758 [doi].

52. Kawano S, Tamura Y, Kojima R, et al. (2018) Structure-function insights into direct lipid transfer between membranes by Mmm1-Mdm12 of ERMES. *J Cell Biol*. 217(3):959-974. doi: 10.1083/jcb.201704119 [doi].

53. Meisinger C, Rissler M, Chacinska A, et al. (2004) The mitochondrial morphology protein Mdm10 functions in assembly of the preprotein translocase of the outer membrane. *Dev Cell*. 7(1):61-71. doi: 10.1016/j.devcel.2004.06.003 [doi].

54. Yamano K, Tanaka-Yamano S, Endo T. (2010) Mdm10 as a dynamic constituent of the TOB/SAM complex directs coordinated assembly of Tom40. *EMBO Rep*. 11(3):187-193. doi: 10.1038/embor.2009.283 [doi].

55. Friedman JR, Lackner LL, West M, DiBenedetto JR, Nunnari J, Voeltz GK. (2011) ER tubules mark sites of mitochondrial division. *Science*. 334(6054):358-362. doi: 10.1126/science.1207385 [doi].

56. Sogo LF, Yaffe MP. (1994) Regulation of mitochondrial morphology and inheritance by Mdm10p, a protein of the mitochondrial outer membrane. *J Cell Biol*. 126(6):1361-1373.

57. Berger KH, Sogo LF, Yaffe MP. (1997) Mdm12p, a component required for mitochondrial inheritance that is conserved between budding and fission yeast. *J Cell Biol*. 136(3):545-553.

58. Park J, Kim Y, Choi S, et al. (2010) Drosophila porin/VDAC affects mitochondrial morphology. *PLoS One*. 5(10):e13151. doi: 10.1371/journal.pone.0013151 [doi].

59. Clancey CJ, Chang SC, Dowhan W. (1993) Cloning of a gene (PSD1) encoding phosphatidylserine decarboxylase from saccharomyces cerevisiae by complementation of an escherichia coli mutant. *Journal of Biological Chemistry*. 268(33):24580-24590.

60. Achleitner G, Gaigg B, Krasser A, et al. (1999) Association between the endoplasmic reticulum and mitochondria of yeast facilitates interorganelle transport of phospholipids through membrane contact. *European Journal of Biochemistry*. 264(2):545-553. https://doi.org/10.1046/j.1432-1327.1999.00658.x. doi: 10.1046/j.1432-1327.1999.00658.x.

61. Daum G, Lees ND, Bard M, Dickson R. (1998) Biochemistry, cell biology and molecular biology of lipids of saccharomyces cerevisiae. *Yeast*. 14(16):1471-1510. https://doi.org/10.1002/(SICI)1097-0061(199812)14:163.0.CO;2-Y. doi: 10.1002/(SICI)1097-0061(199812)14:163.0.CO;2-Y.

62. Birner R, Bürgermeister M, Schneiter R, Daum G. (2001) Roles of phosphatidylethanolamine and of its several biosynthetic pathways in saccharomyces cerevisiae. *Mol Biol Cell*. 12(4):997-1007. https://doi.org/10.1091/mbc.12.4.997. doi: 10.1091/mbc.12.4.997.

63. Gebert N, Joshi AS, Kutik S, et al. (2009) Mitochondrial cardiolipin involved in outer-membrane protein biogenesis: Implications for barth syndrome. *Current Biology*. 19(24):2133-2139. doi: https://doi.org/10.1016/j.cub.2009.10.074.

64. Schlame M, Rua D, Greenberg ML. (2000) The biosynthesis and functional role of cardiolipin. *Progress in Lipid Research*. 39(3):257-288. doi: https://doi.org/10.1016/S0163-7827(00)00005-9
".

65. Gohil VM, Thompson MN, Greenberg ML. (2005) Synthetic lethal interaction of the mitochondrial phosphatidylethanolamine and cardiolipin biosynthetic pathways in saccharomyces cerevisiae. *Journal of Biological Chemistry*. 280(42):35410-35416. doi: 10.1074/jbc.M505478200.

66. Kraft C, Deplazes A, Sohrmann M, Peter M. (2008) Mature ribosomes are selectively degraded upon starvation by an autophagy pathway requiring the Ubp3p/Bre5p ubiquitin protease. *Nat Cell Biol*. 10(5):602-610. doi: 10.1038/ncb1723 [doi].

67. Tuttle DL, Lewin AS, Dunn WA,Jr. (1993) Selective autophagy of peroxisomes in methylotrophic yeasts. *Eur J Cell Biol*. 60(2):283-290.

68. Sakai Y, Koller A, Rangell LK, Keller GA, Subramani S. (1998) Peroxisome degradation by microautophagy in pichia pastoris: Identification of specific steps and morphological intermediates. *J Cell Biol*. 141(3):625-636.

69. Sun Y, Vashisht AA, Tchieu J, Wohlschlegel JA, Dreier L. (2012) Voltage-dependent anion channels (VDACs) recruit parkin to defective mitochondria to promote mitochondrial autophagy. *The Journal of biological chemistry*. 287(48):40652-40660. https://www.ncbi.nlm.nih.gov/pubmed/23060438; https://www.ncbi.nlm.nih.gov/pmc/articles/PMC3504778/. doi: 10.1074/jbc.M112.419721.

70. Suzuki K, Kubota Y, Sekito T, Ohsumi Y. (2007) Hierarchy of atg proteins in pre-autophagosomal structure organization. *Genes Cells*. 12(2):209-218. doi: GTC1050 [pii].

71. Baba M, Osumi M, Scott SV, Klionsky DJ, Ohsumi Y. (1997) Two distinct pathways for targeting proteins from the cytoplasm to the vacuole/lysosome. *J Cell Biol*. 139(7):1687-1695.

72. Xie Z, Nair U, Klionsky DJ. (2008) Atg8 controls phagophore expansion during autophagosome formation. *Mol Biol Cell*. 19(8):3290-3298. doi: 10.1091/mbc.E07-12-1292 [doi].

73. Yan J, Kuroyanagi H, Kuroiwa A, et al. (1998) Identification of mouse ULK1, a novel protein kinase structurally related to C. elegans UNC-51. *Biochem Biophys Res Commun*. 246(1):222-227. doi: S0006291X98985461 [pii].

74. Matsuura A, Tsukada M, Wada Y, Ohsumi Y. (1997) Apg1p, a novel protein kinase required for the autophagic process in saccharomyces cerevisiae. *Gene*. 192(2):245-250. doi: S0378-1119(97)00084-X [pii].

75. Kabeya Y, Kamada Y, Baba M, Takikawa H, Sasaki M, Ohsumi Y. (2005) Atg17 functions in cooperation with Atg1 and Atg13 in yeast autophagy. *Mol Biol Cell*. 16(5):2544-2553. doi: E04-08-0669 [pii].

76. Kamada Y, Funakoshi T, Shintani T, Nagano K, Ohsumi M, Ohsumi Y. (2000) Tor-mediated induction of autophagy via an Apg1 protein kinase complex. *J Cell Biol*. 150(6):1507-1513.

77. Kawamata T, Kamada Y, Kabeya Y, Sekito T, Ohsumi Y. (2008) Organization of the pre-autophagosomal structure responsible for autophagosome formation. *Mol Biol Cell*. 19(5):2039-2050. doi: 10.1091/mbc.E07-10-1048 [doi].

78. Cheong H, Klionsky DJ.(2008) Dual role of Atg1 in regulation of autophagy-specific PAS assembly in saccharomyces cerevisiae. *Autophagy*. 4(5):724-726. doi: 6375 [pii].

79. Reggiori F, Tucker KA, Stromhaug PE, Klionsky DJ. (2004) The Atg1-Atg13 complex regulates Atg9 and Atg23 retrieval transport from the pre-autophagosomal structure. *Dev Cell*. 6(1):79-90. doi: S1534-5807(03)00402-7 [pii].

80. Mizushima N. (2010) The role of the Atg1/ULK1 complex in autophagy regulation. *Curr Opin Cell Biol*. 22(2):132-139. doi: 10.1016/j.ceb.2009.12.004 [doi].

81. Nakatogawa H, Suzuki K, Kamada Y, Ohsumi Y. (2009) Dynamics and diversity in autophagy mechanisms: Lessons from yeast. *Nat Rev Mol Cell Biol*. 10(7):458-467. doi: 10.1038/nrm2708 [doi].

82. Nakatogawa H, Ohbayashi S, Sakoh-Nakatogawa M, et al. (2012) The autophagy-related protein kinase Atg1 interacts with the ubiquitin-like protein Atg8 via the Atg8 family interacting

motif to facilitate autophagosome formation. *Journal of Biological Chemistry*. 287(34):28503-28507. doi: 10.1074/jbc.C112.387514.

83. Hardie DG, Ross FA, Hawley SA. (2012) AMPK: A nutrient and energy sensor that maintains energy homeostasis. *Nat Rev Mol Cell Biol*. 13(4):251-262. doi: 10.1038/nrm3311 [doi].

84. Mayer FV, Heath R, Underwood E, et al. (2011) ADP regulates SNF1, the saccharomyces cerevisiae homolog of AMP-activated protein kinase. *Cell Metab*. 14(5):707-714. doi: 10.1016/j.cmet.2011.09.009 [doi].

85. McCartney RR, Schmidt MC. (2001) Regulation of Snf1 kinase. activation requires phosphorylation of threonine 210 by an upstream kinase as well as a distinct step mediated by the Snf4 subunit. *J Biol Chem*. 276(39):36460-36466. doi: 10.1074/jbc.M104418200 [doi].

86. Oakhill JS, Steel R, Chen ZP, et al. (2011) AMPK is a direct adenylate charge-regulated protein kinase. *Science*. 332(6036):1433-1435. doi: 10.1126/science.1200094 [doi].

87. Amodeo GA, Rudolph MJ, Tong L. (2007) Crystal structure of the heterotrimer core of saccharomyces cerevisiae AMPK homologue SNF1. *Nature*. 449(7161):492-495. doi: nature06127 [pii].

88. Kim J, Kundu M, Viollet B, Guan KL. (2011) AMPK and mTOR regulate autophagy through direct phosphorylation of Ulk1. *Nat Cell Biol*. 13(2):132-141. doi: 10.1038/ncb2152 [doi].

89. Kim J, Kim Y, Fang C, et al. (2013) Differential regulation of distinct Vps34 complexes by AMPK in nutrient stress and autophagy. *Cell*. 152(1):290-303. doi: https://doi.org/10.1016/j.cell.2012.12.016.

90. Yi C, Tong J, Lu P, et al. (2017) Formation of a Snf1-Mec1-Atg1 module on mitochondria governs energy deprivation-induced autophagy by regulating mitochondrial respiration. *Dev Cell*. 41(1):59-71.e4. doi: S1534-5807(17)30160-0 [pii].

91. Vozza A, Blanco E, Palmieri L, Palmieri F. (2004) Identification of the mitochondrial GTP/GDP transporter in saccharomyces cerevisiae. *Journal of Biological Chemistry*. 279(20):20850-20857. doi: 10.1074/jbc.M313610200.

92. Mao K, Wang K, Zhao M, Xu T, Klionsky DJ. (2011) Two MAPK-signaling pathways are required for mitophagy in saccharomyces cerevisiae. *J Cell Biol*. 193(4):755-767. doi: 10.1083/jcb.201102092 [doi].

93. Martin H, Arroyo J, Sanchez M, Molina M, Nombela C. (1993) Activity of the yeast MAP kinase homologue Slt2 is critically required for cell integrity at 37 degrees C. *Mol Gen Genet*. 241(1-2):177-184.

94. Westfall PJ, Ballon DR, Thorner J. (2004) When the stress of your environment makes you go HOG wild. *Science*. 306(5701):1511-1512. doi: 306/5701/1511 [pii].

95. Paravicini G, Friedli L. (1996) Protein-protein interactions in the yeast PKC1 pathway: Pkc1p interacts with a component of the MAP kinase cascade. *Mol Gen Genet*. 251(6):682-691.

96. Kanki T, Wang K, Cao Y, Baba M, Klionsky DJ. (2009) Atg32 is a mitochondrial protein that confers selectivity during mitophagy. *Dev Cell*. 17(1):98-109. doi: 10.1016/j.devcel.2009.06.014 [doi].

97. Okamoto K, Kondo-Okamoto N, Ohsumi Y. (2009) Mitochondria-anchored receptor Atg32 mediates degradation of mitochondria via selective autophagy. *Dev Cell*. 17(1):87-97. doi: 10.1016/j.devcel.2009.06.013 [doi].

98. Harding TM, Morano KA, Scott SV, Klionsky DJ. (1995) Isolation and characterization of yeast mutants in the cytoplasm to vacuole protein targeting pathway. *J Cell Biol*. 131(3):591-602.

99. Aoki Y, Kanki T, Hirota Y, et al. (2011) Phosphorylation of serine 114 on Atg32 mediates mitophagy. *Mol Biol Cell*. 22(17):3206-3217. doi: 10.1091/mbc.E11-02-0145 [doi].

100. Noda NN, Ohsumi Y, Inagaki F. (2010) Atg8-family interacting motif crucial for selective autophagy. *FEBS Lett*. 584(7):1379-1385. doi: 10.1016/j.febslet.2010.01.018 [doi].

101. Kaufmann A, Beier V, Franquelim HG, Wollert T. (2014) Molecular mechanism of autophagic membrane-scaffold assembly and disassembly. *Cell*. 156(3):469-481. doi: 10.1016/j.cell.2013.12.022 [doi].

102. Kaufmann A, Wollert T. (2014) Scaffolding the expansion of autophagosomes. *Autophagy*. 10(7):1343-1345. doi: 10.4161/auto.28980 [doi].

103. Westermann B, Neupert W. (2000) Mitochondria-targeted green fluorescent proteins: Convenient tools for the study of organelle biogenesis in saccharomyces cerevisiae. *Yeast*. 16(15):1421-1427. https://doi.org/10.1002/1097-0061(200011)16:153.0.CO;2-U. doi: 10.1002/1097-0061(200011)16:153.0.CO;2-U.

104. Alberti S, Gitler AD, Lindquist S. (2007) A suite of gateway cloning vectors for high-throughput genetic analysis in saccharomyces cerevisiae. *Yeast (Chichester, England)*. 24(10):913-919. https://www.ncbi.nlm.nih.gov/pubmed/17583893; https://www.ncbi.nlm.nih.gov/pmc/articles/PMC2190539/. doi: 10.1002/yea.1502.

105. Gnaiger E. (2005) High-resolution respirometry for the study of mitochondrial function in health and disease. the OROBOROS oxygraph-2k.23:6-6.

106. Sales S, Knittelfelder O, Shevchenko A. (2017) Lipidomics of human blood plasma by high-resolution shotgun mass spectrometry. In: Greening DW, Simpson RJ, eds. *Serum/plasma proteomics: Methods and protocols.* New York, NY: Springer New York; 203-212. https://doi.org/10.1007/978-1-4939-7057-5_16. 10.1007/978-1-4939-7057-5_16.

107. Sales S, Graessler J, Ciucci S, et al. (2016) Gender, contraceptives and individual metabolic predisposition shape a healthy plasma lipidome. *Scientific Reports*. 6:27710. https://doi.org/10.1038/srep27710.

108. Schuhmann K, Almeida RF, Baumert MF, Herzog R FAU - Bornstein, Stefan,R., FAU BS, Shevchenko A. (2012) Shotgun lipidomics on a LTQ orbitrap mass spectrometer by successive switching between acquisition polarity modes. *Journal of mass spectrometry : JMS JID - 9504818*.

109. Schuhmann K, Thomas H, Ackerman JM, Nagornov KO, Tsybin YO, Shevchenko AA. (2017) Intensity-independent noise filtering in FT MS and FT MS/MS spectra for shotgun lipidomics. *Analytical chemistry JID - 0370536*.

110. Schuhmann K, Srzentic K, Nagornov KO, et al. (2017) Monitoring membrane lipidome turnover by metabolic (15)N labeling and shotgun ultra-high-resolution orbitrap fourier transform mass spectrometry. *Analytical chemistry JID - 0370536*.

111. Herzog R, Schuhmann KF, Schwudke D FAU - Sampaio, Julio,L., et al. (2012) LipidXplorer: A software for consensual cross-platform lipidomics. *PloS one JID - 101285081*.

112. Jazwinski SM, Kriete A. (2012)The yeast retrograde response as a model of intracellular signaling of mitochondrial dysfunction. *Frontiers in physiology*. 3:139-139. https://www.ncbi.nlm.nih.gov/pubmed/22629248; https://www.ncbi.nlm.nih.gov/pmc/articles/PMC3354551/. doi: 10.3389/fphys.2012.00139.

113. Pujol-Carrion N, Petkova MI, Serrano L, de la Torre-Ruiz MA. (2013) The MAP kinase Slt2 is involved in vacuolar function and actin remodeling in saccharomyces cerevisiae mutants affected by endogenous oxidative stress. *Appl Environ Microbiol*. 79(20):6459-6471. doi: 10.1128/AEM.01692-13.

114. Burgess SM, Delannoy M, Jensen RE. (1994) MMM1 encodes a mitochondrial outer membrane protein essential for establishing and maintaining the structure of yeast mitochondria. *J Cell Biol*. 126(6):1375. http://jcb.rupress.org/content/126/6/1375.abstract. doi: 10.1083/jcb.126.6.1375.

115. Berger KH, Sogo LF, Yaffe MP. (1997) Mdm12p, a component required for mitochondrial inheritance that is conserved between budding and fission yeast. *J Cell Biol*. 136(3):545. http://jcb.rupress.org/content/136/3/545.abstract. doi: 10.1083/jcb.136.3.545.

116. Sogo LF, Yaffe MP. (1994) Regulation of mitochondrial morphology and inheritance by Mdm10p, a protein of the mitochondrial outer membrane. *J Cell Biol*. 126(6):1361. http://jcb.rupress.org/content/126/6/1361.abstract. doi: 10.1083/jcb.126.6.1361.

117. Yeh JI, Chinte U, Du S. (1998) Structure of glycerol-3-phosphate dehydrogenase, an essential monotopic membrane enzyme involved in respiration and metabolism. *Proc Natl Acad Sci USA*. 105(9):3280-3285. doi: 10.1073/pnas.0712331105.

118. DeRisi JL, Iyer VR, Brown PO. (1997) Exploring the metabolic and genetic control of gene expression on a genomic scale. *Science*. 278(5338):680. http://science.sciencemag.org/content/278/5338/680.abstract. doi: 10.1126/science.278.5338.680.

119. McMaster CR, Bell RM. (1994) Phosphatidylcholine biosynthesis via the CDP-choline pathway in saccharomyces cerevisiae. multiple mechanisms of regulation. *Journal of Biological Chemistry*. 269(20):14776-14783.

120. Traven A, Wong JMS, Xu D, Sopta M, Ingles CJ. (2001) Interorganellar communication: ALTERED NUCLEAR GENE EXPRESSION PROFILES IN A YEAST MITOCHONDRIAL DNA MUTANT. *Journal of Biological Chemistry*. 276(6):4020-4027. doi: 10.1074/jbc.M006807200.

121. Osman C, Voelker DR, Langer T. (2011) Making heads or tails of phospholipids in mitochondria. *J Cell Biol*. 192(1):7. http://jcb.rupress.org/content/192/1/7.abstract. doi: 10.1083/jcb.201006159.